applied sciences

MDPI

Article

Study on the Uncertainty of Input Variables in Seismic Fragility Curves Based on the Number of Ground Motions

Sangki Park *, Dongwoo Seo, Kyusan Jung and Jaehwan Kim

Department of Structural Engineering Research, Korea Institute of Civil Engineering and Building Technology, Goyang 10223, Republic of Korea; dwseo@kict.re.kr (D.S.); jungkyusan@kict.re.kr (K.J.); jaehwankim@kict.re.kr (J.K.)
* Correspondence: skpark@kict.re.kr

Abstract: Seismic fragility curves, derived from ground motion data, are essential tools for predicting and assessing potential damage to structures during earthquakes. Seismic fragility curves are vital for assessing the structural behavior of buildings and establishing disaster response criteria when an earthquake occurs. We performed an incremental dynamic analysis based on 400 ground motion data. We sampled various sets of ground motions (10, 20, 30, 40, 50, 60, 70, 80, 90, 100, 150, 200, 250, 300, and 350) and derived seismic fragility curves for three performance criteria, based on inter-story drift, by conducting 100,000 simulations for two steel frame structures each (6-story and 13-story). Fewer ground motions increase the uncertainty of the seismic fragility curve, distorting the results. Conversely, increasing the number of ground motions improves the reliability of the input variables and enhances the consistency of the results. The median and the logarithmic standard deviation for both structures converged toward the reference values when 30 or more ground motions were used. Similar results were observed when $\geq$50 ground motions were used. Specifically, more ground motions corresponded with a lower uncertainty in deriving the input variables for the seismic fragility curve, improving the reliability of the results. In conclusion, the number of ground motions used is directly related to the computational time for numerical analysis when deriving seismic fragility curves. Therefore, considering an appropriate number of ground motions is crucial to enhancing the reliability of the input variables used in evaluating the structural performance.

Keywords: ground motions; seismic fragility curves; earthquake damage

check for updates

Citation: Park, S.; Seo, D.; Jung, K.; Kim, J. Study on the Uncertainty of Input Variables in Seismic Fragility Curves Based on the Number of Ground Motions. *Appl. Sci.* **2024**, *14*, 11787. https://doi.org/10.3390/app142411787

Academic Editor: Sang-Hyo Kim

Received: 15 November 2024
Revised: 5 December 2024
Accepted: 11 December 2024
Published: 17 December 2024

Copyright: © 2024 by the authors. Licensee MDPI, Basel, Switzerland. This article is an open access article distributed under the terms and conditions of the Creative Commons Attribution (CC BY) license (https://creativecommons.org/licenses/by/4.0/).

1. Introduction

Earthquakes are unpredictable natural disasters that occur frequently worldwide. Earthquakes such as the 1989 Loma Prieta Earthquake in the U.S. (MW 6.9), the 1994 Great Hanshin Earthquake in Japan (MW 6.9), the 1995 Chi-Chi Earthquake in Taiwan (MW 7.7), the 2004 Indian Ocean Earthquake and Tsunami (MW 9.2–9.3), and the 2011 Great East Japan Earthquake (MW 9.0–9.1) caused substantial human and material damage [1].

Seismic fragility curves estimate the conditional probability of structural damage based on the response of a building to an earthquake. They are used to assess and predict damage to facilities caused by earthquakes [2–4]. They estimate the probability of damage to target facilities by considering earthquake intensity measures (IMs), such as peak ground acceleration (PGA) and spectral acceleration, from various ground motion records. This estimation allows for damage assessments of facilities affected by earthquakes [4,5]. Typically, the characteristics and geographic location of the facility are analyzed to determine the type and number of input ground motions and IMs required. Nonlinear numerical analysis is then performed, and the results are used to generate seismic fragility curves. Determining the number of input ground motions and the type of earthquake intensity to be used in the dynamic numerical analysis of the target facility is crucial at this point [6].

Shinozuka et al. proposed empirical seismic fragility curves using bridge damage data from the 1995 Kobe Earthquake. They also performed nonlinear analysis on typical bridges

in Memphis, U.S., and used the results to present numerical analysis-based seismic fragility curves [4]. Baker suggested a method for deriving effective numerical analysis-based seismic fragility curves using dynamic structural analysis results [7]. Park et al. derived seismic fragility curves for a 7-span continuous steel box girder bridge and 2 transmission towers (154 kV and 765 kV) by considering 27 ground motions (20 overseas-measured, 3 domestic-measured ground motions, and 4 artificial ground motions), accounting for Korean ground behavior [8]. Jeon et al. assessed the seismic fragility of a 15-story non-seismic design reinforced concrete shear wall apartment building, designed in the mid-1980s, using 30 ground motions and evaluating four performance levels [9]. Jin-Young Kim and Tae-Wan Kim assessed the seismic fragility of a two-story piloti structure using incremental dynamic analysis (IDA), considering four ground conditions with twenty-eight ground motion pairs based on seven pairs of ground motions [10]. Sofia et al. derived seismic fragility curves for 5 performance levels using 33 ground motions for 4 prestressed concrete road bridges in Chile [11]. Dumova-Jovanoska conducted a seismic fragility analysis for 6- and 16-story reinforced concrete structures. Two-hundred-and-forty synthetic ground motions were generated and used to assess seismic fragility for five damage levels for the Skopje area [12]. Kappos and Panagopoulos performed seismic fragility analyses for five damage levels on various concrete buildings (2-, 4-, and 9-story) in Greece using 16 ground motions [13]. Su et al. analyzed seismic fragility for three damage levels on unreinforced masonry buildings (3-, 4-, 5-, and 6-story) using First Order Second Moment, Latin Hypercube Sampling (LHS), Monte Carlo Simulation (MCS) methods, and IDA. They used 20 measured ground motions from the PEER DB and performed seismic fragility analysis by increasing the ground motion magnitude from 0.05 g to 0.8 g in increments of 0.05 g PGA [14]. Blasi et al. performed seismic fragility analysis for unreinforced, masonry-reinforced, and composite-reinforced concrete structures using 20 ground motions [15].

This reveals that in many studies related to seismic fragility curves, a wide range of ground motion counts are used for seismic fragility analysis, and no clear definition exists regarding the appropriate number of ground motions.

Eads et al. examined various aspects related to the computation of the mean annual frequency of collapse and showed that the mean annual frequency of collapse is dominated by earthquake ground motion intensities. Also, it was shown that uncertainty in the collapse fragility curve and mean annual frequency of collapse can be expressed as a function of the number of ground motions used in calculations [16]. Ruggieri et al. presented on the seismic fragility of 15 RC school buildings built between 1960 and 1980s in Southern Italy. In their study, a practical mode for application of the multi-stripe analyses was proposed and SPO2FRAG v1.1(beta) software was used to predict the median and the record-to-record variability of the seismic response of an SDOF system, and to provide the fragility curves for each limit state [17]. Nettis et al. proposed a framework for efficient risk assessment of multi-span girder bridges considering knowledge-based uncertainties. From a case study, it addressed issues such as the use of optimal intensity measures, the required number of model realizations and discrepancies with respect to accurate nonlinear time history analysis [18]. Li et al. proposed an alternative time-dependent seismic fragility assessment framework for aging highway bridges. In the study, they pointed out that the variation in the peak value of seismic response may result from the couple contributions of the uncertainty of ground motions and modeling related parameters [19].

Bovo and Buratti studied epistemic uncertainty in the relationship between material constitutive models and seismic fragility curves for reinforced concrete structures, analyzing two design options for the girders and columns of steel structures by considering various material model variables. Seismic fragility curves were derived for three performance levels using IDA with 30 ground motions [20]. Hofer et al. conducted a study on epistemic uncertainty regarding IMs, damage classification criteria, target facility selection methods, and seismic fragility generation methods for damage caused by tornadoes in the Joplin, Missouri, area [21].

Recent advancements in technology, including increased computing power, have made it possible to perform numerical analyses on large and complex structures that used to be difficult to handle, allowing for seismic fragility analysis with many ground motions. The appropriate number of ground motions must first be determined when using methods such as IDA, which is widely used for generating seismic fragility curves. Afterward, different magnitudes of ground motions are selected, and numerical analysis is performed on combinations of the number and magnitude of ground motions, considering damage levels to generate the fragility curves [22,23]. Seismic fragility refers to the probabilistic vulnerability of a structure to ground motion variability. If the number of ground motions is insufficient, the diversity of the ground motions is inadequately considered, distorting the fragility results. Conversely, considering numerous ground motions increases the diversity of the ground motions and improves the accuracy of the fragility curves; however, it requires an excessively long analysis time. Therefore, when generating seismic fragility curves, the number of ground motions used is directly linked to the numerical analysis time, making it crucial to consider an appropriate number and magnitude of ground motions.

Ground motions used in seismic fragility curves are key input variables in seismic vulnerability analysis and inherently involve uncertainty in the numerical model of the target facility and the selection of input ground motions. Epistemic uncertainty, arising from limitations in knowledge and data, can significantly impact the reliability of seismic fragility curves. This study derived seismic fragility curves by considering many ground motions and analyzed the relationship between the key input variables of the fragility curves and the number of ground motions used in generating the fragility curves. A quantitative analysis was conducted using statistical techniques to address the epistemic uncertainty associated with the varying number of ground motions.

For this purpose, two steel special moment frame structures were used as example facilities, and combinations of different numbers of ground motions (10, 20, 30, 40, 50, 60, 70, 80, 90, 100, 150, 200, 250, 300, and 350) were selected from 400 ground motions for nonlinear dynamic analysis. Based on the analysis results, seismic fragility curves were generated for three damage levels, and a statistical analysis was conducted on the relationship between the fragility curves and the number of ground motions considered.

2. Types and Characteristics of Ground Motions

The ground motions used in this study were referenced from the set of ground motions used in FEMA P-695 [24]. In FEMA P-695, ground motions are classified as “Far-Field” if the epicentral distance is 10 km or more and “Near-Field” if it is less than 10 km. “Near-Field” motions are further divided into “Pulse” and “Non-Pulse” types. The data from the PEER NGA Database were used; 400 ground motions were selected, considering the “Pulse” and “Non-Pulse” types of “Near-Field” motions and “Far-Field” motions, per the conditions specified in FEMA P-695. The 400 ground motions consist of 200 near-field motions and 200 far-field motions. The selection criteria are followed: (1) magnitude ranging from M6.5 to M8.0 for both the near-field and the far-field ground motions and (2) site–source distance, i.e., Rrup and Rjb, ranging from 0 km to 10 km for the near-field and from 10 km to 1000 km for the far-field ground motions. Figure 1 illustrates the distribution of the 400 ground motions, with an average PGA of 0.2547 g. Table 1 summarizes the range of characteristics of the ground motions.

Table 1. Min/Max values of ground motion parameters.

Parameter	Min. Value	Max. Value	Avg. Value
Magnitude, Mw	6.5	7.9	7.11
Peak Ground Acceleration, PGA (m/s)	0.01	1.49	0.25
Arias Intensity, IA (m/s)	0.1	26.10	2.33
Soil preferred shear-velocity, Vs30 (m/s)	133.11	2016.13	408.30
Joyner-Boore distance to rupture plane, Rjb (km)	0.07	349.57	70.13

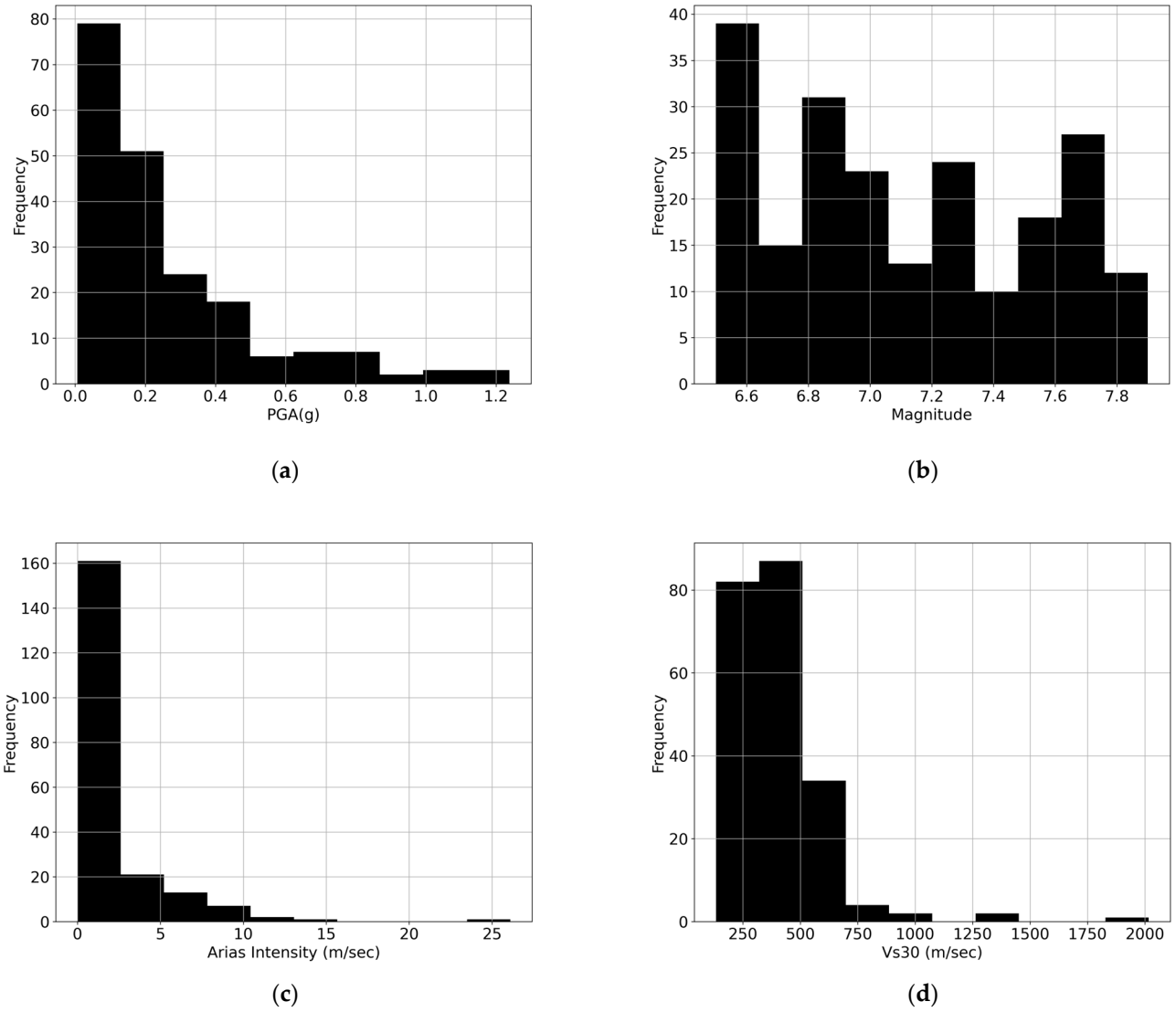

Figure 1. Statistical characteristics of ground motions. (**a**) Histogram of peak ground acceleration; (**b**) histogram of magnitude; (**c**) histogram of arias intensity; (**d**) histogram of vs30.

3. Seismic Fragility Theory

Seismic fragility curves are widely used for structural safety assessments, seismic performance evaluations, and establishing disaster response standards to mitigate earthquake damage [25]. These fragility curves provide quantitative damage levels for given performance levels based on the magnitude of the input seismic load, making them a widely used method for the performance evaluation of structures. Based on seismic analysis results, the probability of damage for a given earthquake magnitude can be calculated and expressed using a log-normal distribution function. The median and log-standard deviation of the log-normal distribution function can be calculated using the maximum likelihood estimation, as shown in Equation (1).

$$L = \prod_{i=1}^{N} [F(a_i)]^{x_i} [1 - F(a_i)]^{1-x_i}. \quad (1)$$

Here, $F(\cdot)$ represents the seismic fragility curve, and a_i is the input earthquake magnitude (PGA). x_i takes a value of $x_i = 1$ if damage occurs at the ith instance; otherwise, it

takes a value of $x_i = 0$. N is the number of ground motions. The seismic fragility curve can be expressed as a cumulative distribution function, as shown in Equation (2) [4,26].

$$F(a) = \Phi\left[\frac{\ln\left(\frac{a}{\theta}\right)}{\beta}\right]. \quad (2)$$

Here, a represents the input variable, the earthquake magnitude (PGA), θ is the median, β is the log-standard deviation, and $\Phi[\cdot]$ is the cumulative probability function of the standard normal distribution.

Various methods have been proposed for deriving seismic fragility curves. Techniques such as multiple stripe analysis, IDA, and cloud analysis are commonly used; this study employed the IDA method for deriving the seismic fragility curves. IDA is a popular method enabling toe estimation of the structural performance under various seismic loads. The main goal of IDA is to determine the relationship between the seismic intensity level, i.e., IM, and the corresponding engineering demand, i.e., structural response. The IDA can be explained with the following steps: (1) selecting a set of seismic ground motions; (2) selecting the appropriate intensity measure (IM) and engineering demand measure (EDM); and (3) scaling the selected the seismic ground motions, i.e., IM, and performing the nonlinear structural analysis using finite element method to obtain the structural response, i.e., EDM. Once structural analysis using IDA is completed, the constructing fragility curves can be estimated by optimization techniques to obtain two parameters of the fragility curves [14,22,23,26,27]. In this study, the magnitude of the ground motions considered for the fragility curve input ranged from 0.01 g to 5.00 g in increments of 0.01 g.

4. Analysis of the Relationship Between the Number of Input Ground Motions and Seismic Fragility

4.1. Example Facility: Six-Story Commercial Building

A seismic fragility analysis was performed on a six-story steel special moment frame structure designed in 1976 [28–30]. The target facility, located in California, U.S., was designed according to the 1973 Uniform Building Code (UBC). The building has a rectangular plan measuring 36.6 m × 36.6 m, with floors consisting of an 8.2 cm-thick lightweight concrete slab and a 7.5 cm metal deck, and the building height is 25.3 m. The structure is a moment frame, with internal frames designed to resist gravity loads. The main structural members use A-36 steel, with a yield stress assumed to be 303 MPa. The first natural period is 1.40 s, and the total weight of the building, excluding live loads, was calculated to be approximately 3533 tons (34,644 kN), consistent with the results presented by Anderson and Bertero [31].

Figure 2 illustrates the front and plan views, along with the sizes of the beams and columns. Numerical analysis for the target facility was performed using Opensees V3.7.0, software widely used for dynamic analysis of structures [32]. A 2D numerical model was developed, considering the symmetry of the structure, with the model constructed using nonlinear beam–column elements and fiber sections. Regarding using a 2D numerical model instead of a 3D numerical model for the target facility, Kunnath et al. [28] and Kalkan and Kunnath [29] developed 2D and 3D numerical models for the target facility and performed numerical analyses on both. For symmetric structures such as the target facility, a 2D numerical model was developed using half of the assigned mass for each component based on the 3D model. Two- and three-dimensional models of the six-story commercial building were calibrated to give the best match of the first-model period. Then, a comparative analysis of the structural responses from the 2D and 3D numerical models revealed identical responses. Detailed calibration of the numerical model can be found in works by Kunnath et al. [28] and Kalkan and Kunnath [29]. Therefore, this study used a 2D numerical model instead of a 3D model for the numerical analysis. More detailed information on the six-story structure can be found in Table 2.

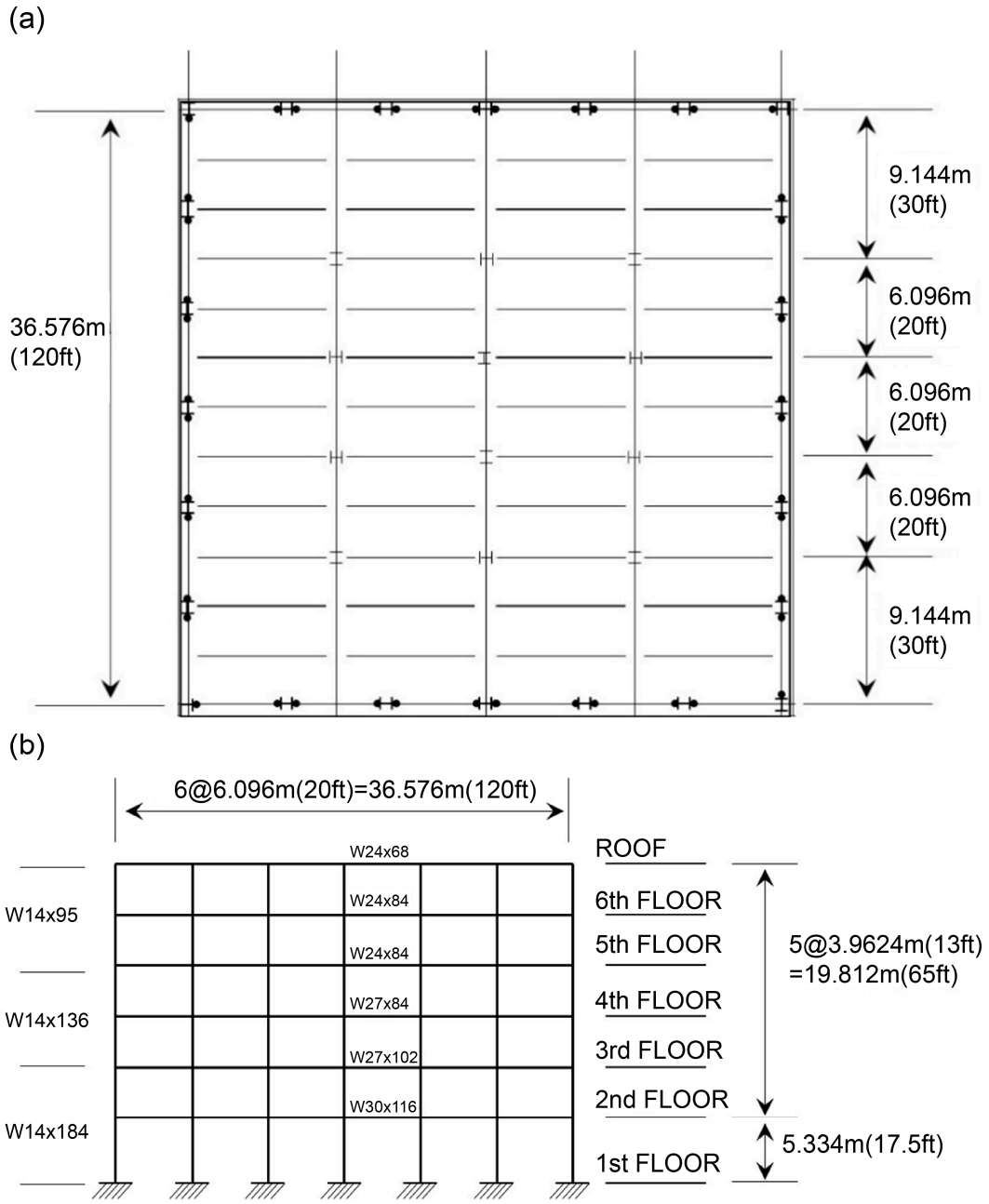

Figure 2. Plan and front views of the six-story building. (**a**) Plan view of target building. (**b**) Front view of target building.

Table 2. Detailed information on the numerical model of the six-story building.

Item	Type	Model	Parameter
Element	Beam	nonlinearBeamColumn	Node I & J, 4 integer points, Section ID
	Column	nonlinearBeamColumn	Node I & J, 4 integer points, Section ID
Section	Fiber Section	fiberSec	3 patch quadr with no. of fibers and section properties
Material	uniaxialMaterial	Steel01(Bilinear)	E(20GPa), fy(303MPa), b(0.03)

For the time history analysis, the Newmark-beta method, which is a popular method of numerical integration, is adopted with 5% Rayleigh damping. Also, average constant acceleration ($\gamma = 0.5$ and $\beta = 0.25$) is used to obtain the stability.

IDA was performed on the target facility using 400 ground motions, considering the ground motion magnitudes (PGA, with 0.01 g increments from 0.01 g to 5.0 g). Based on the structural response at the top floor, seismic fragility curves were derived for three performance levels (Table 3) [33].

Table 3. Performance level and inter-story drift ratio of the six-story building.

Performance Level	Inter-Story Drift Ratio (%)	Value
1—Immediate Occupancy (IO)	0.7	0.1760 m (6.93 inches)
2—Life Safety (LS)	2.5	0.6287 m (24.75 inches)
3—Collapse Prevention (CP)	5.0	1.2573 m (49.50 inches)

Figure 3 illustrates the derived fragility curves for the three performance levels. The black solid line represents performance level 1 with a median of 0.30 g, the blue dashed line represents performance level 2 with 0.96 g, and the red dotted line represents performance level 3 with 1.01 g. These values were used as reference values (Table 4).

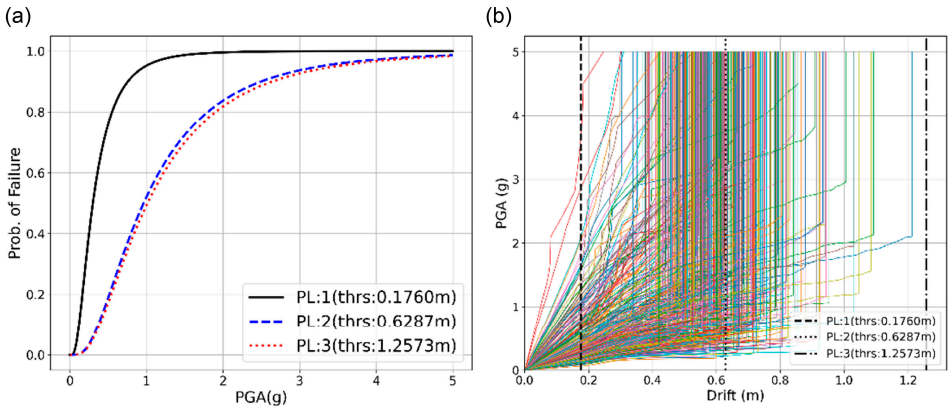

Figure 3. Seismic fragility curve and displacement distribution of the six-story building. (**a**) Fragility curves; (**b**) Max. displacements.

Table 4. Parameters of seismic fragility curves of the six-story building.

Performance Level	Median (g)	STD	PGA at 16% Level (g)	PGA at 84% Level (g)
1—IO	0.3000	0.7237	0.1461	0.6161
2—LS	0.9638	0.7430	0.4603	2.0177
3—CP	1.0148	0.7471	0.4828	2.1334

Ground motion samples of 10, 20, 30, 40, 50, 60, 70, 80, 90, 100, 150, 200, 250, 300, and 350 were randomly selected from 400 ground motions to analyze the relationship between the number of ground motions considered in calculating seismic fragility curves and the variables of the fragility curves. A statistical analysis of the fragility curve input variables was performed after repeating the process 100,000 times for each sample size. Sampling methods such as MCS and LHS are commonly used in engineering experiments. MCS, which randomly selects samples, is easily implemented and can be applied to various problems. However, it is inefficient and requires many samples to produce reliable results. Conversely, LHS distributes samples uniformly by dividing the sample space of the target variables evenly. This method allows for a more effective distribution of samples and can produce high-quality results with relatively fewer samples. Therefore, the LHS method was chosen for sampling the ground motions in this study [34–36].

Ten ground motions were randomly selected from the 400 ground motions, and the variables for the seismic fragility curves were calculated for the three performance levels (Figure 4 and Table 5). Figure 3 and Table 4 present the reference values, where the median

is 0.30 g for Performance Level 1. When 10 ground motions were selected and the seismic fragility curve was derived (repeated 100,000 times), the median ranged from 0.14 g to 0.79 g, with an average of 0.31 g, representing a 2.06% difference from the reference value. Additionally, the reference value is 0.72 for the log-standard deviation, with a minimum of 0.15, a maximum of 1.30, and an average of 0.68, resulting in a 6.43% difference from the reference value.

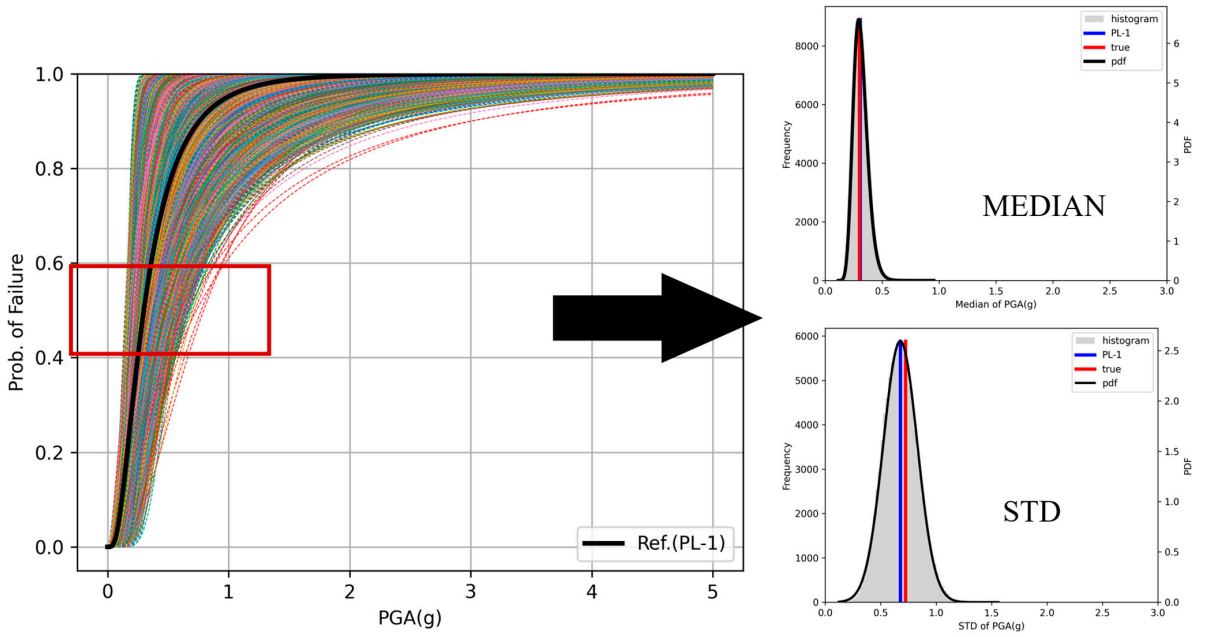

(**a**)

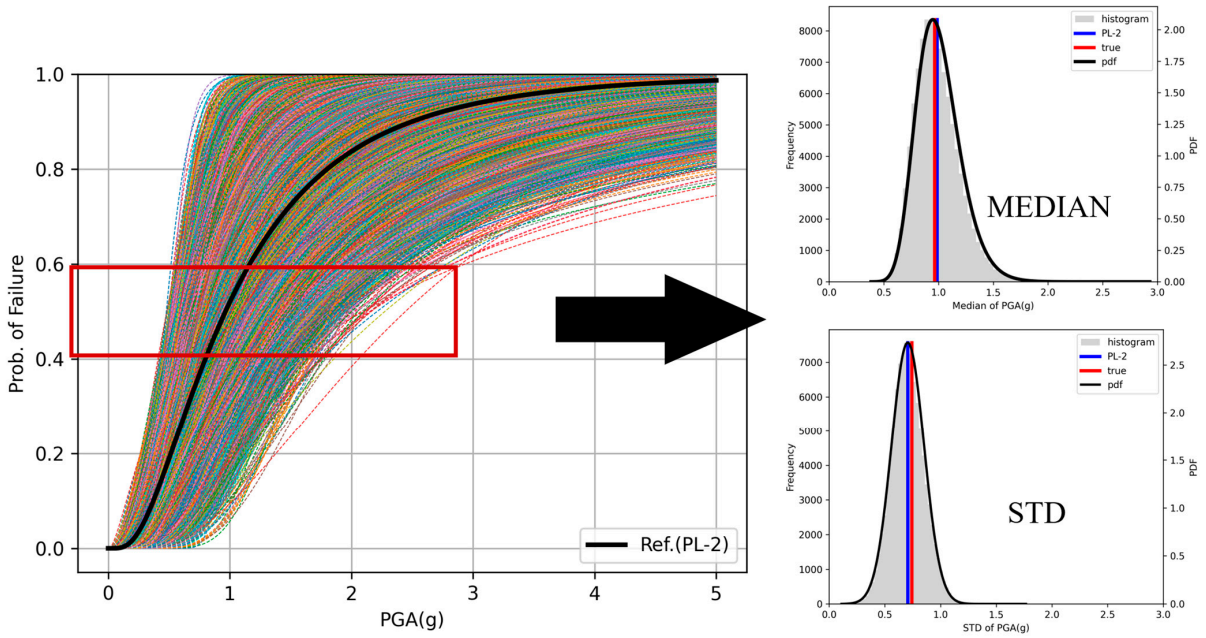

(**b**)

Figure 4. *Cont.*

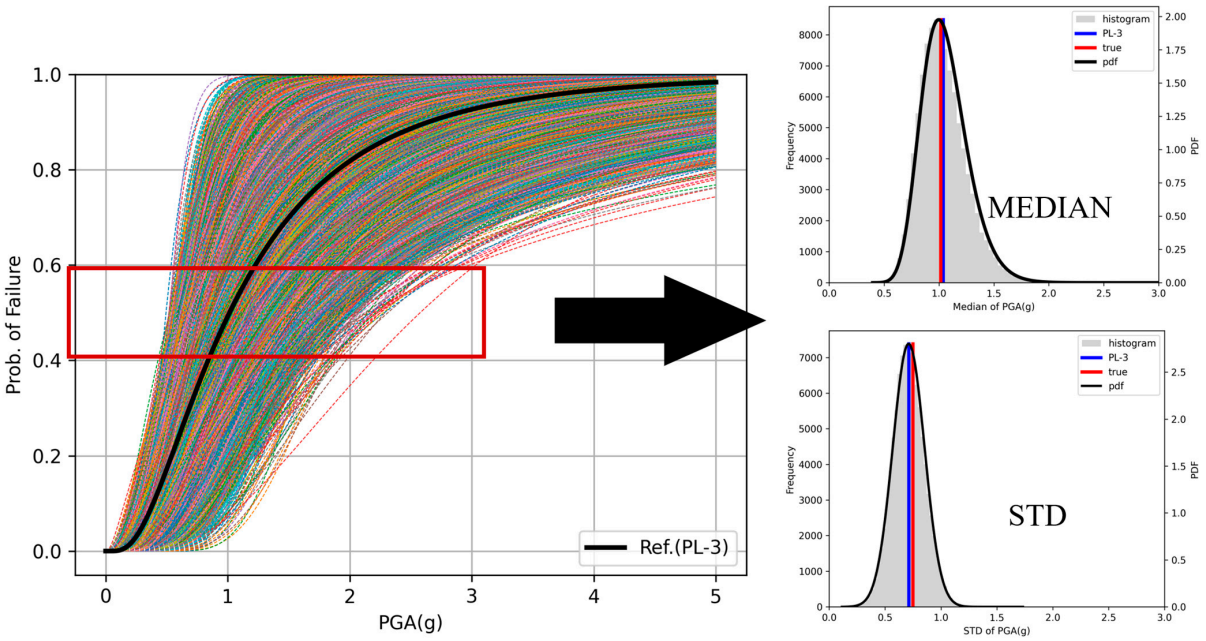

(**c**)

Figure 4. Seismic fragility curves and histograms of the six-story building (N = 10). (**a**) Performance Level 1; (**b**) Performance Level 2; (**c**) Performance Level 3.

Table 5. Seismic fragility curve parameters range of the six-story building (N = 10).

Performance Level	Median (g)				Difference (%)
	Ref	Min	Max	Avg	
1—IO	0.3000	0.1442	0.7947	0.3062	2.0638
2—LS	0.9638	0.4782	2.4424	0.9850	2.2061
3—CP	1.0148	0.4944	2.5765	1.0371	2.1951
Level	Log-standard deviation				Difference (%)
	Ref	Min	Max	Avg	
1—IO	0.7237	0.1542	1.3016	0.6771	6.4377
2—LS	0.7430	0.1387	1.4723	0.7059	4.9873
3—CP	0.7471	0.1421	1.4444	0.7107	4.8720

The left graph in Figure 4 presents the results of the seismic fragility analysis, with the solid line representing the median of the fragility curve calculated after 100,000 repetitions. The right graph displays the frequency distribution and probability density function for the mean (top right graph) and the log-standard deviation (bottom right graph) of the results; the red solid line represents the reference value, the blue solid line represents the mean, and the black solid line represents the results after 100,000 repetitions.

Seismic fragility curves were calculated for the 16%, 50%, and 84% levels using the results from selecting 10 ground motions at random based on the values presented in Table 5 and summarized at Table 6.

For Performance Level 1, the 16% fragility level ranged from 0.04 g to 0.68 g, revealing a variation of over 17 times (Table 5). At the 84% fragility level, it ranged from 0.17 g to 2.90 g, exhibiting a variation of over 17 times. These differences can cause overestimation or underestimation when using fragility curve values for further analysis, such as vulnerability assessments of target facilities, cost evaluations for earthquake damage, or seismic performance analyses of structures.

The same analysis was performed considering 20 and 30 ground motions, respectively. Figure 5 and Table 7 summarize the results for 20 ground motions. Figure 6 and Table 8 present the results for 30 ground motions.

Table 6. Seismic fragility curve calculation results for Performance Level 1.

Performance Level—1		PGA (g) of Target Probability of Failure			Note
Median	**STD**	**16%**	**50%**	**84%**	
Minimum	Minimum	0.1237	0.1442	0.1682 (min)	
	Average	0.0736	0.1442	0.2828	
	Maximum	0.0395 (min)	0.1442	0.5263	
Average	Minimum	0.2626	0.3062	0.3569	
	Average	0.1561	0.3062	0.6003	
	Maximum	0.0839	0.3062	1.1171	
Maximum	Minimum	0.6817 (max)	0.7947	0.9264	
	Average	0.4053	0.7947	1.5582	
	Maximum	0.2178	0.7947	2.8996 (max)	

Table 7. Seismic fragility curve parameters range of the six-story building (N = 20).

Performance Level	Median (g)				Difference (%)
	Ref	**Min**	**Max**	**Avg**	
1—IO	0.3000	0.1745	0.5159	0.3027	0.9235
2—LS	0.9638	0.5136	1.7285	0.9730	0.9577
3—CP	1.0148	0.5544	1.7872	1.0245	0.9507
Performance Level	Log-standard deviation				Difference (%)
	Ref	Min	Max	Avg	
1—IO	0.7237	0.2925	1.1117	0.7038	2.7410
2—LS	0.7430	0.3365	1.2521	0.7282	1.9919
3—CP	0.7471	0.3586	1.2527	0.7326	1.9378

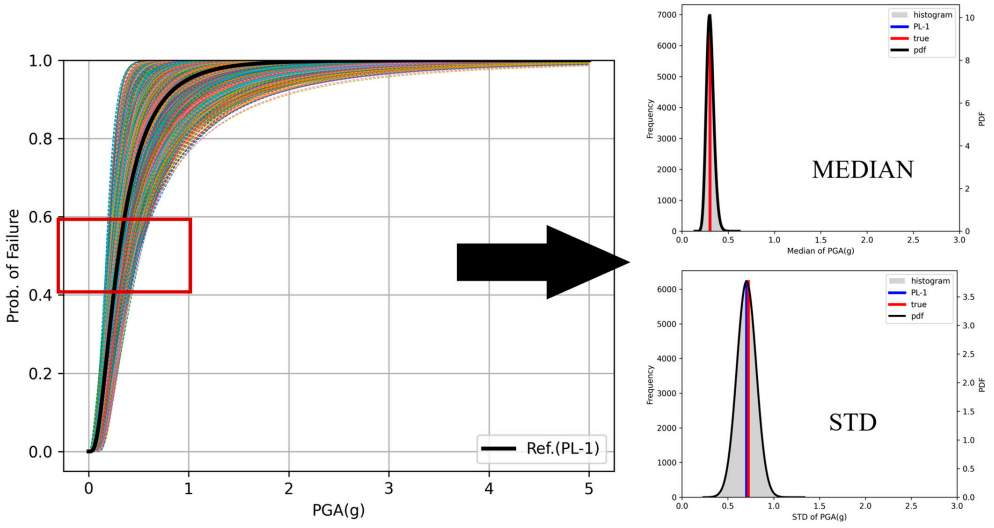

(**a**)

Figure 5. *Cont.*

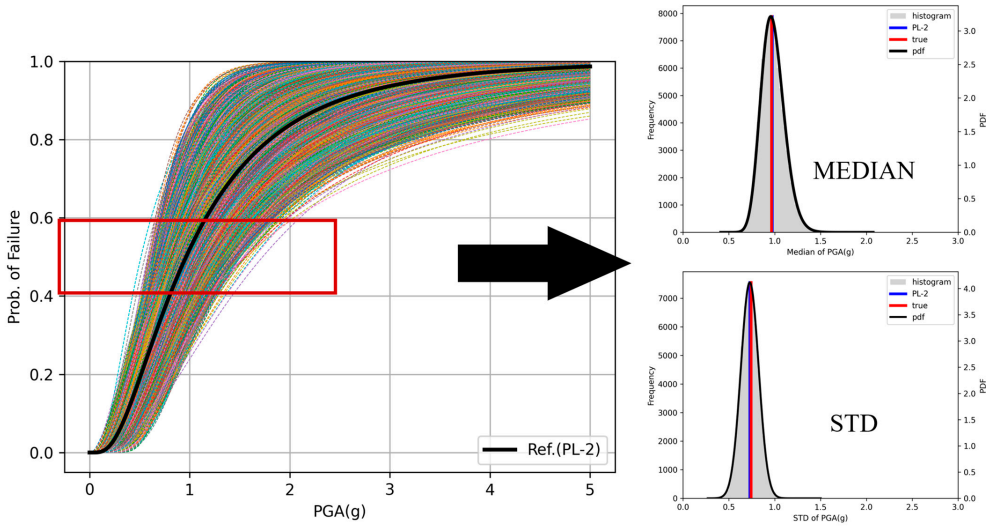

(**b**)

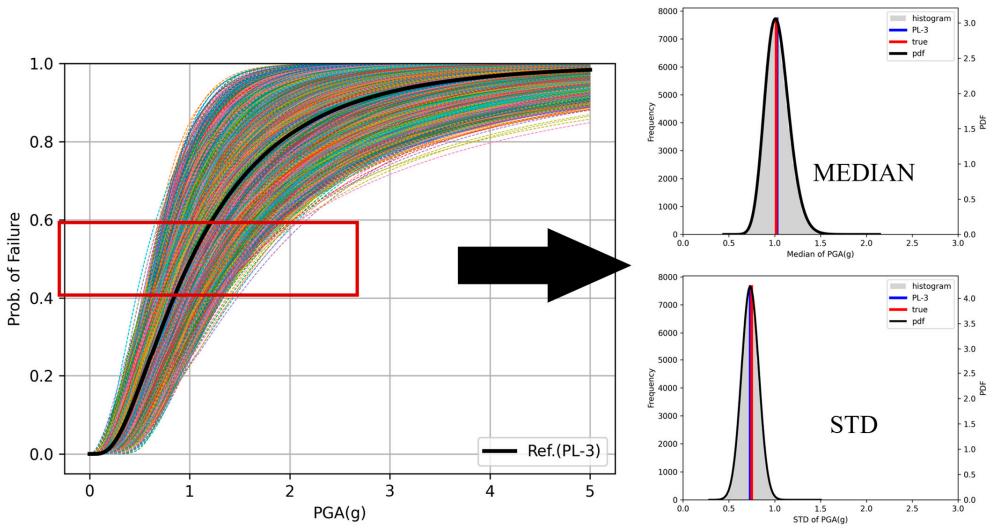

(**c**)

Figure 5. EDS spectrum analysis of 17-4PH (**a**), 316L (**b**), and 304 (**c**).

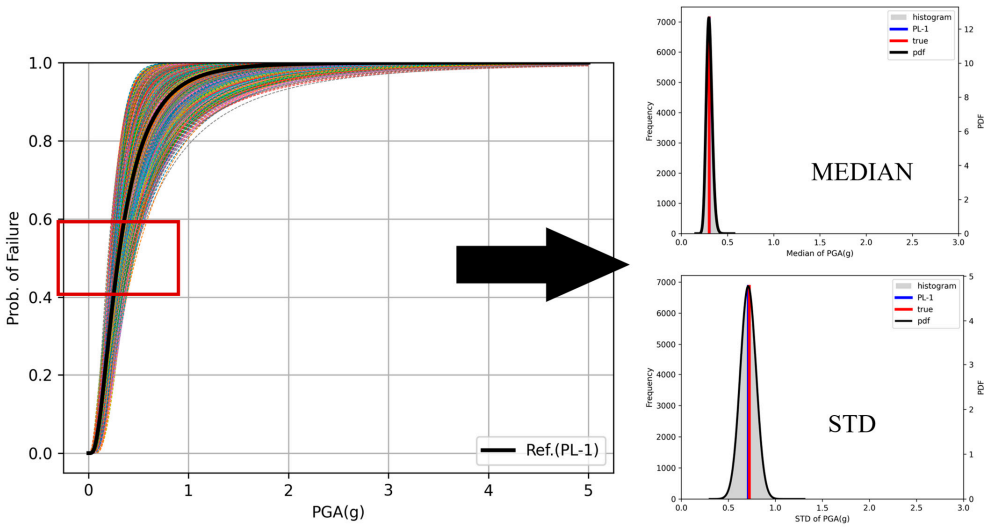

(**a**)

Figure 6. *Cont*.

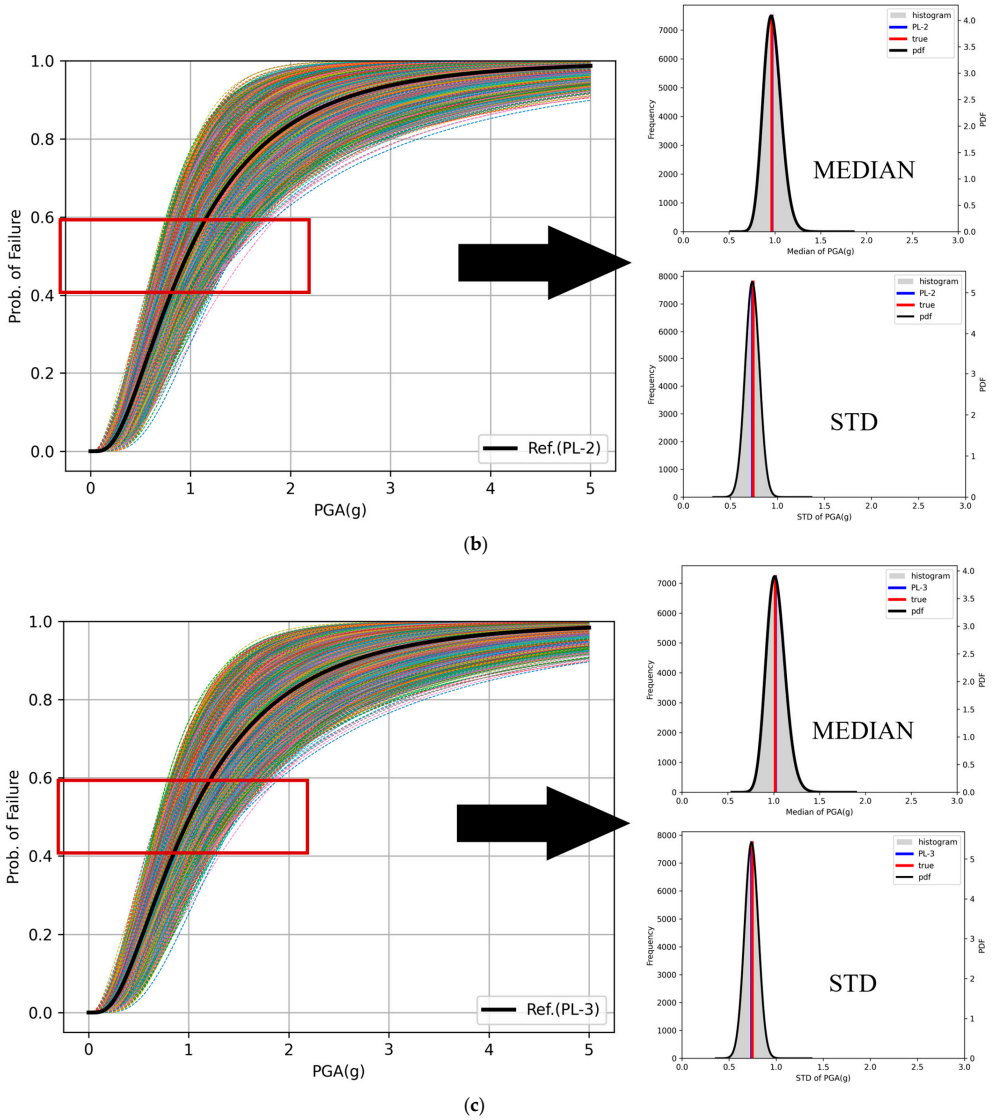

Figure 6. EDS spectrum analysis of 17-4PH (**a**), 316L (**b**), and 304 (**c**).

Table 8. Seismic fragility curve parameters range of the six-story building (N = 30).

Performance Level	Median (g)				Difference (%)
	Ref	Min	Max	Avg	
1—IO	0.3000	0.1946	0.4747	0.3015	0.4959
2—LS	0.9638	0.6463	1.5458	0.9689	0.5290
3—CP	1.0148	0.6802	1.5781	1.0201	0.5158
Performance Level	Log-standard deviation				Difference (%)
	Ref	Min	Max	Avg	
1—IO	0.7237	0.3770	1.0909	0.7112	1.7229
2—LS	0.7430	0.3989	1.1347	0.7338	1.2345
3—CP	0.7471	0.4493	1.1461	0.7381	1.2081

As the number of considered ground motions gradually increases, the frequency distribution becomes a smoother bell-shaped curve (Figures 4–6), indicating that the distribution of the seismic fragility input variables tends to follow a normal distribution. Additionally, the range of minimum and maximum values for each performance level decreases, implying that the input variables of the fragility curve converge toward the reference

values as the number of ground motions considered in the seismic fragility curve increases (Tables 5, 7 and 8). This indicates that the results can be distorted if few ground motions are considered.

Furthermore, the same analysis was performed considering 50, 100, 200, 300, and 350 ground motions. As the number of ground motions increases, the difference between the fragility curve input variables and the reference values decreases. Table 9 and Figure 7 present the results for 50 and 350 ground motions, respectively.

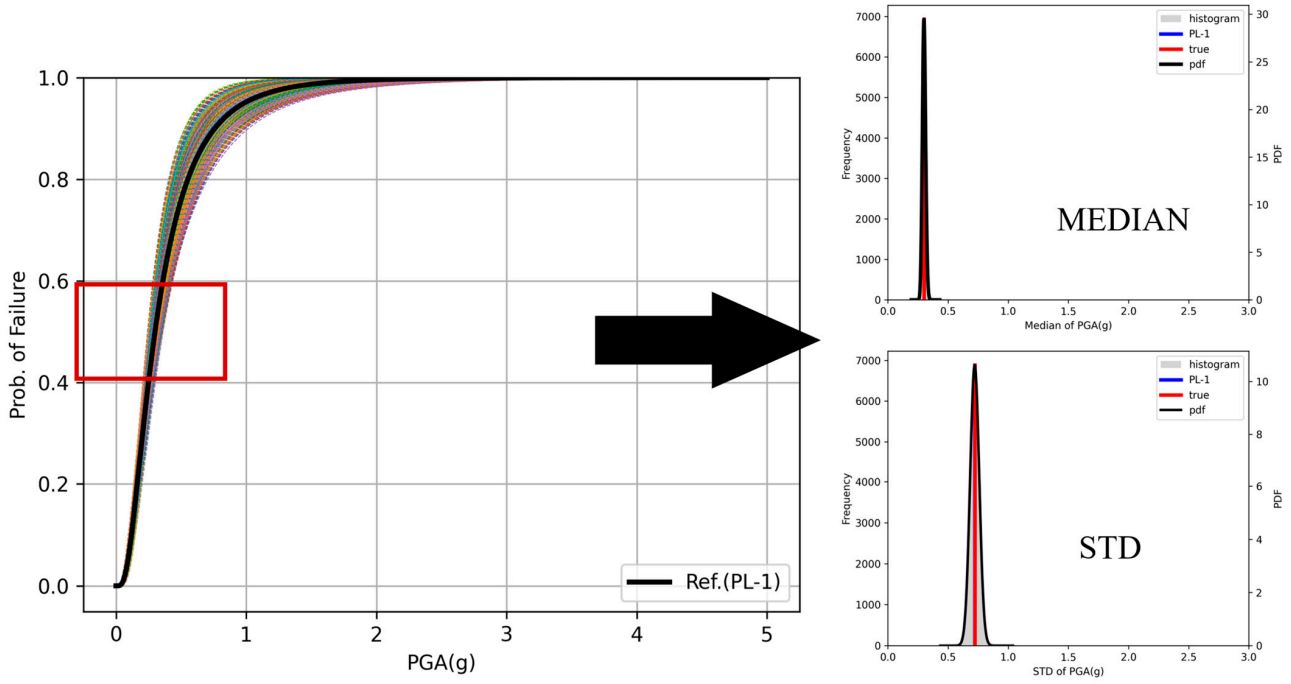

(**a**)

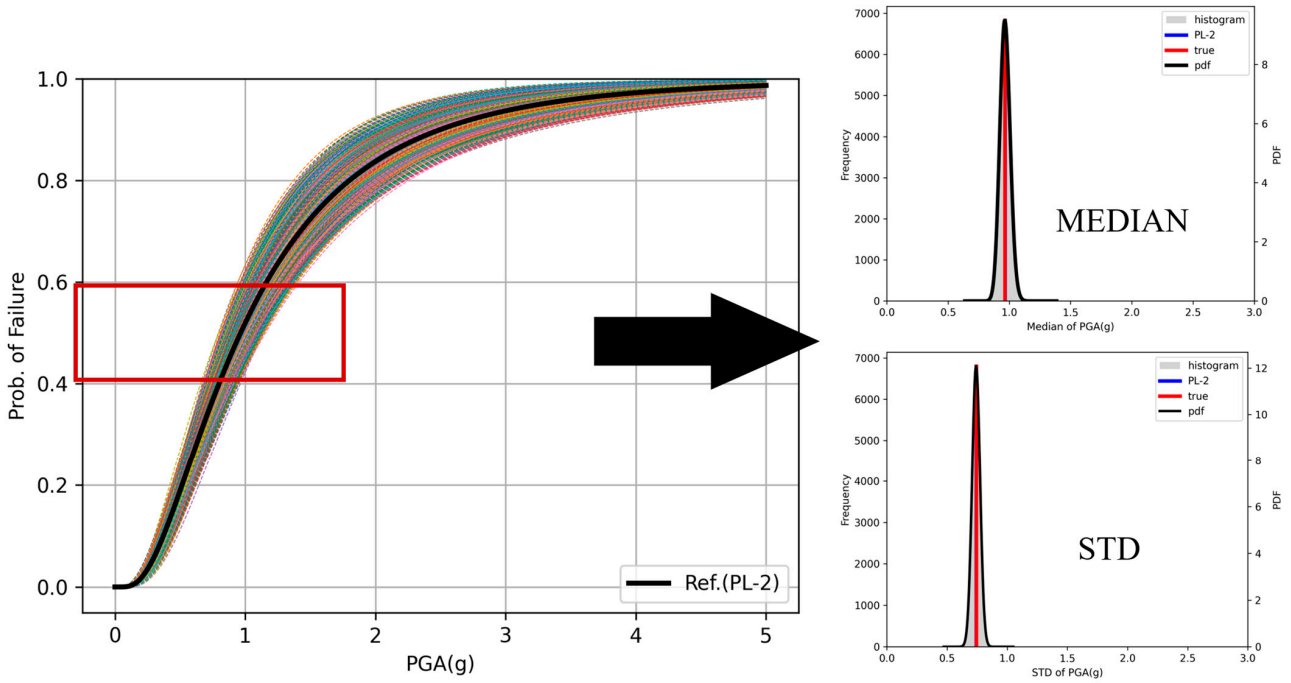

(**b**)

Figure 7. *Cont.*

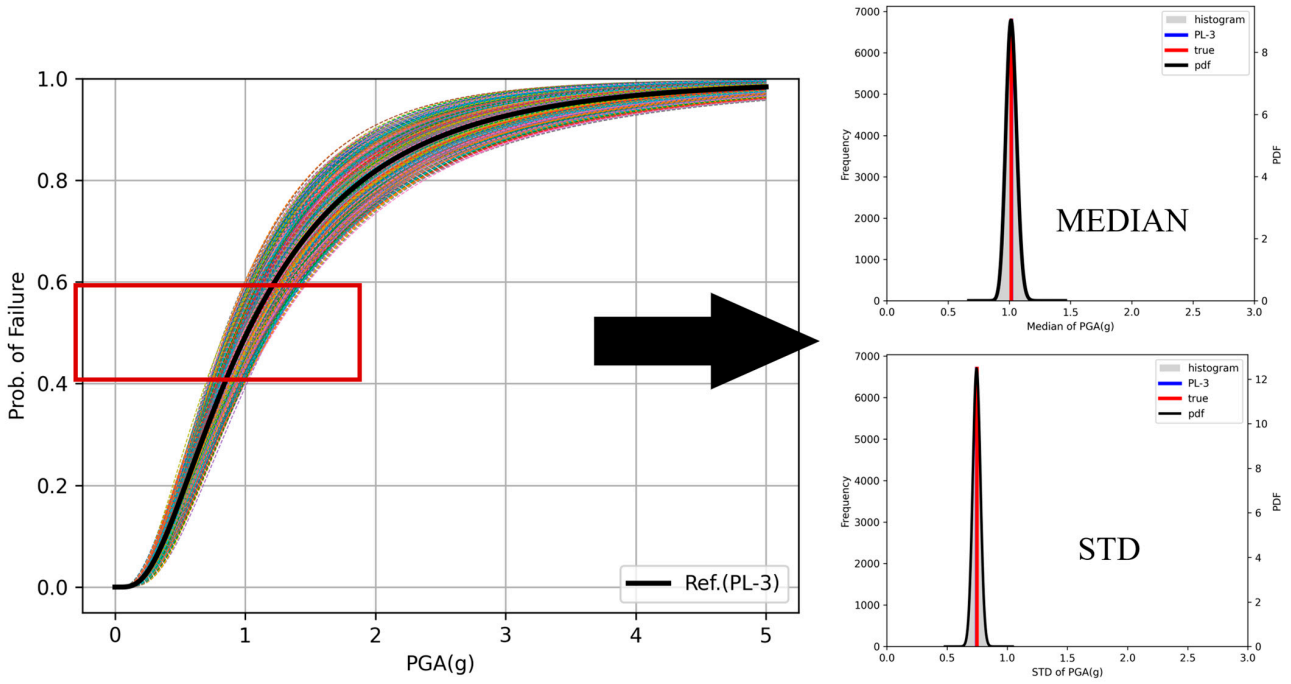

(**c**)

Figure 7. Seismic fragility curves and histograms of the six-story building (N = 350). (**a**) Performance Level 1; (**b**) Performance Level 2; (**c**) Performance Level 3.

Table 9. Seismic fragility curve parameter range of the six-story building (N = 50).

Performance Level	Median (g)				Difference (%)
	Ref	Min	Max	Avg	
1—IO	0.3000	0.2265	0.4294	0.3007	0.2449
2—LS	0.9638	0.7248	1.3300	0.9663	0.2605
3—CP	1.0148	0.7718	1.3920	1.0175	0.2599
Performance Level	Log-standard deviation				Difference (%)
	Ref	Min	Max	Avg	
1—IO	0.7237	0.4670	0.9978	0.7169	0.9379
2—LS	0.7430	0.4886	1.0060	0.7383	0.6331
3—CP	0.7471	0.4903	1.0074	0.7425	0.6123

Figure 8 illustrates the difference between the mean values of each fragility input variable and the reference values for the three performance levels. When 30 or more ground motions were considered, the difference in the median value from the reference value was about 0.47%, 0.47%, and 0.44% and about 0.50%, 0.50%, and 0.47% for the log-standard deviation at each performance level. When 50 or more ground motions were considered, the difference in the median decreased to about 0.34%, 0.32%, and 0.31% for each performance level, and when 100 or more were considered, it decreased to 0.20%, 0.19%, and 0.19% for each performance level. For the log-standard deviation, the difference decreased to 0.37%, 0.35%, and 0.35% for each performance level with 50 ground motions and to 0.23%, 0.19%, 0.19%, and 0.26% for each performance level with 100 ground motions. The values converge toward the reference values as the number of considered ground motions increases.

This difference between the two fragility parameters indicates that using few ground motions when generating fragility curves can lead to overestimation during subsequent analyses, such as vulnerability assessments, cost evaluations, or seismic performance assessments. Thus, the number of ground motions considered in fragility curve generation is critical.

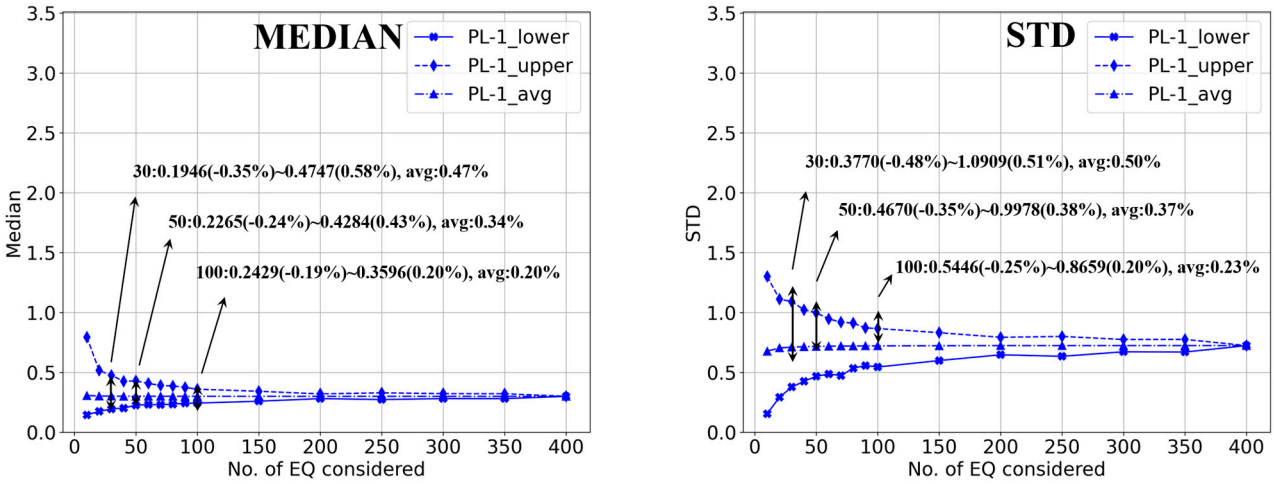

(**a**)

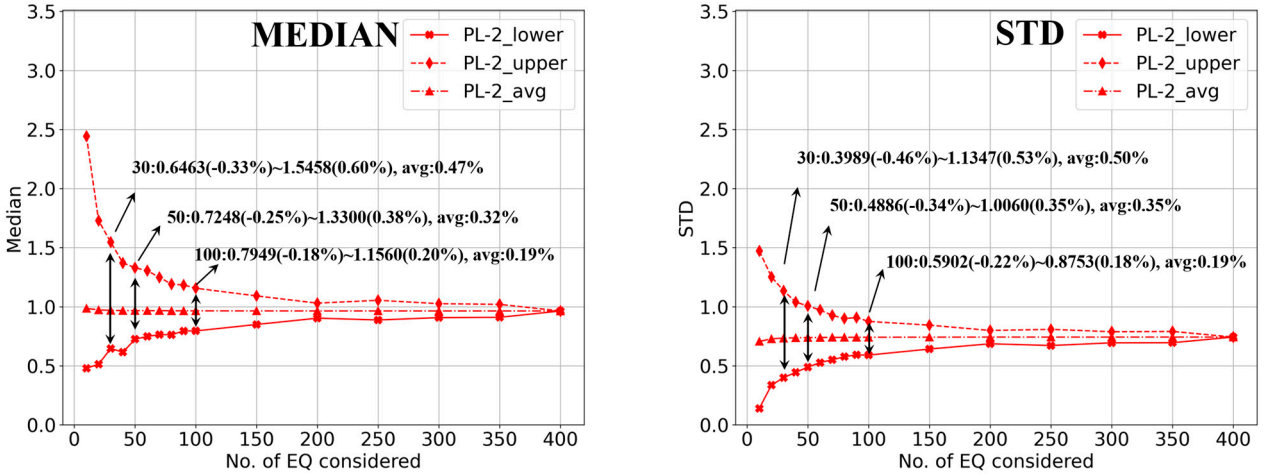

(**b**)

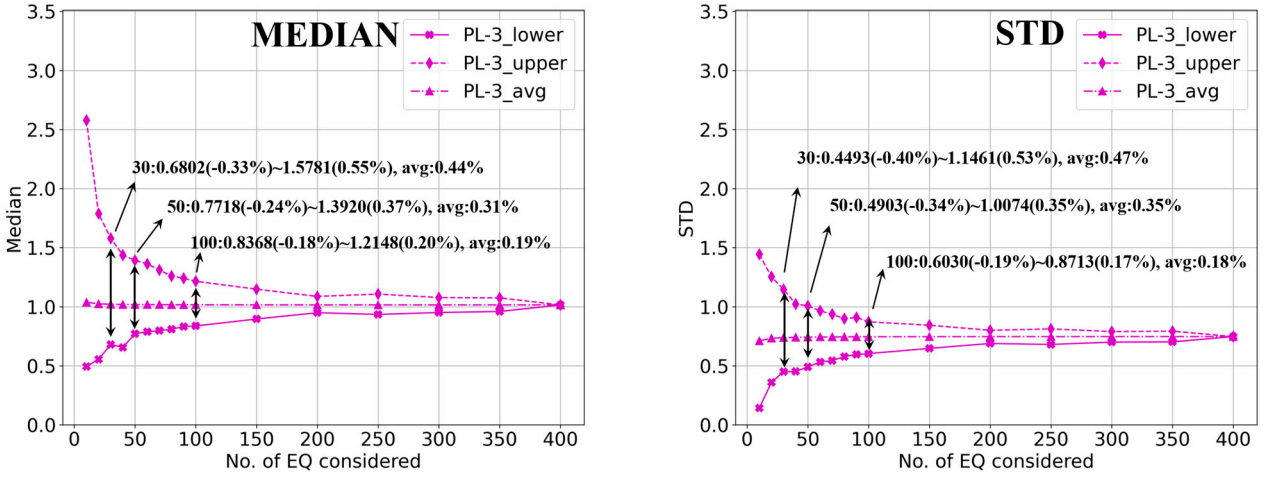

(**c**)

Figure 8. No. of ground motions vs. Difference of the six-story building. (**a**) Performance Level 1; (**b**) Performance Level 2; (**c**) Performance Level 3.

4.2. Example Facility: 13-Story Commercial Building

The second example facility is a 13-story steel special moment frame structure with one basement level and 13 above-ground floors [28–30]. The facility is located in California, U.S., and was designed based on the 1973 UBC and constructed in 1975. The facility has a rectangular plan measuring 48.8 m × 48.8 m, with a height of 57.45 m. The structure is a moment frame, with internal frames designed to resist gravity loads [28–30,37]. The first natural period is 3.04 s.

Figure 9 illustrates the front and plan views, along with the sizes of the beams and columns. Similar to the previous example, the target facility was analyzed using a 2D numerical model. For the 13-story structure, the same three performance levels were considered as for the six-story structure [33]. Figure 10 presents the results of the seismic fragility curves for the three performance levels; the black line represents Performance Level 1 with a median of 0.4137 g, the blue dashed line represents Performance Level 2 with 1.1322 g, and the red dotted line represents Performance Level 3 with 1.2440 g, all of which were assumed as reference values (Table 10).

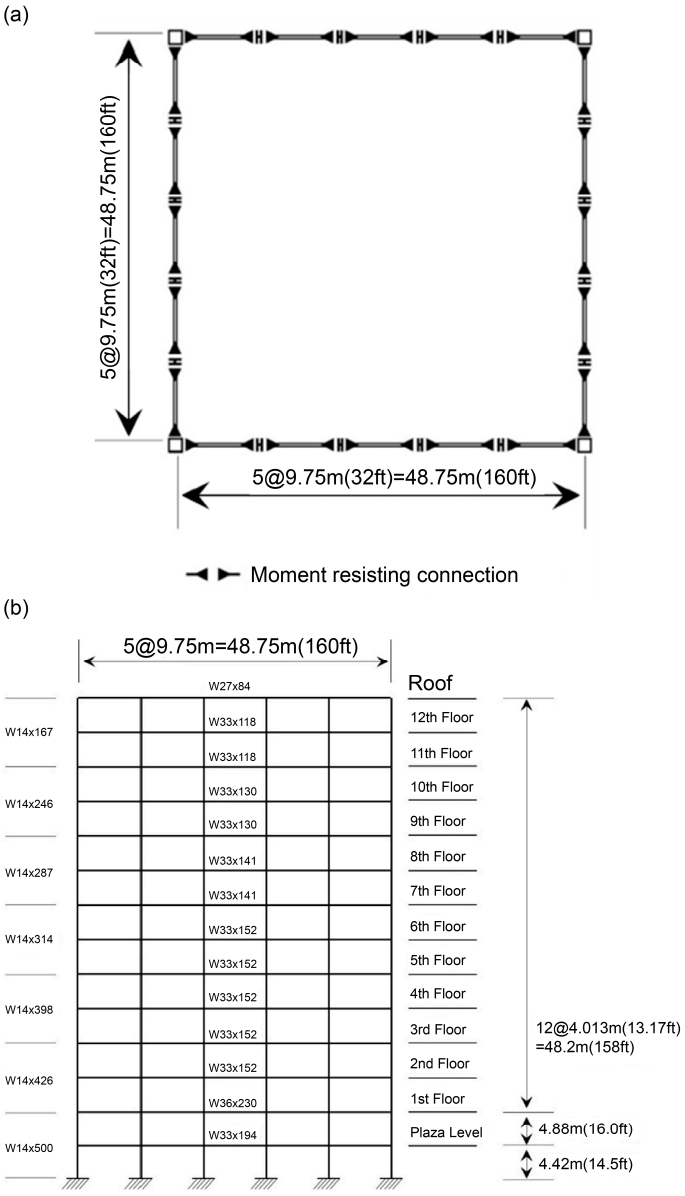

Figure 9. Plan and front views of the 13-story building. (**a**) Plan view of target building; (**b**) front view of target building.

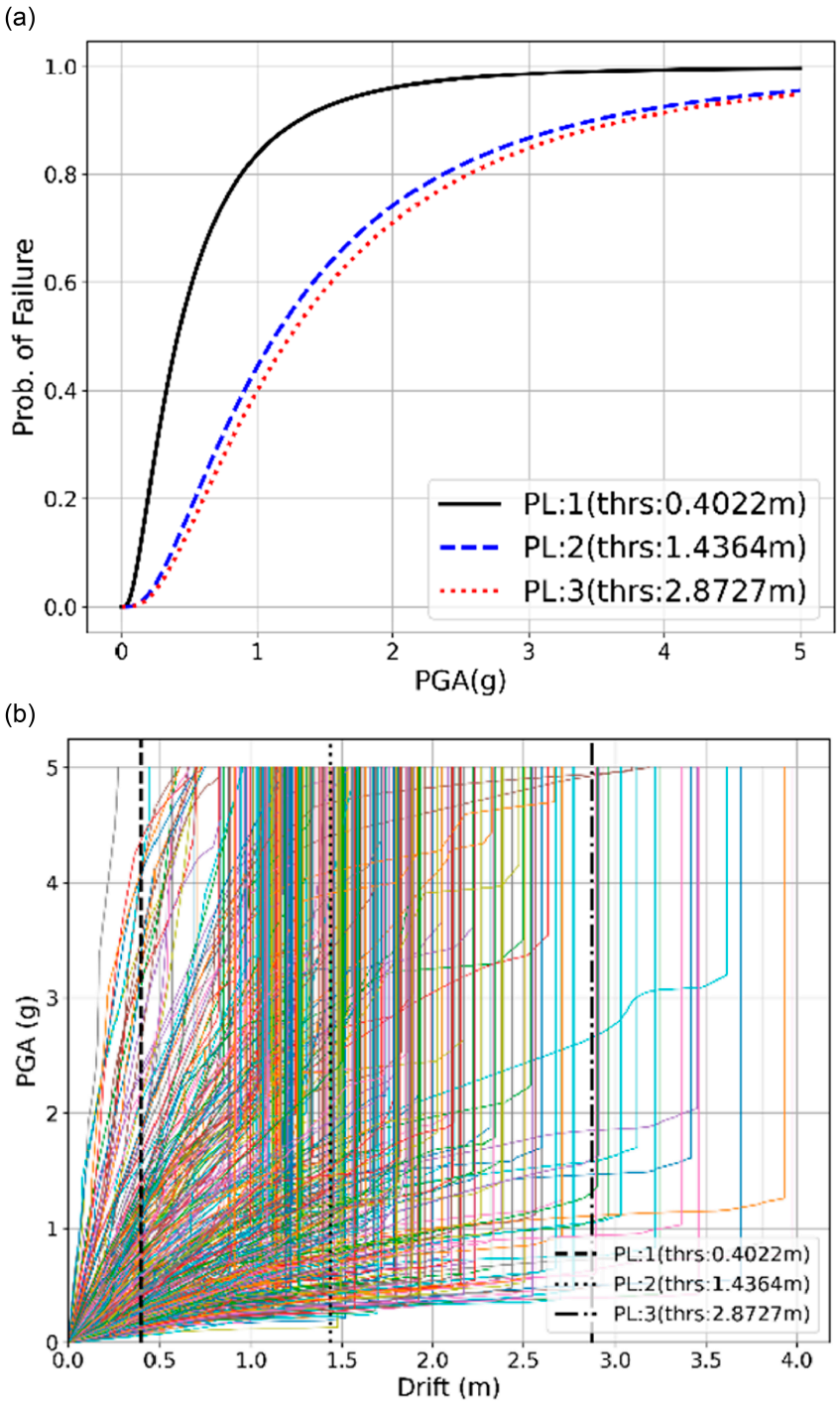

Figure 10. Seismic fragility curve of the thirteen-story building. (**a**) Fragility curves; (**b**) Max. displacements.

Table 10. Parameters of seismic fragility curve of the thirteen-story building.

Performance Level	Median (g)	STD	PGA at 16% Level (g)	PGA at 84% Level (g)
1—IO	0.4137	0.9013	0.1688	1.0139
2—LS	1.1322	0.8779	0.4729	2.7105
3—CP	1.2440	0.8568	0.5306	2.9165

Similar to the six-story example, LHS was used to select ground motions for various sizes of samples from the total 400 ground motions. The seismic fragility curve variables were statistically analyzed after repeating the process 100,000 times for each sample size.

When considering 10 ground motions, the variables for the fragility curve for the three performance levels were calculated (Figure 11), and a comparison was made with the reference values presented in Table 10. For Performance Level 1 (immediate occupancy), the reference median value was 0.41 g. When 10 ground motions were randomly selected and the fragility curve was derived (after 100,000 repetitions), the median ranged from 0.17 g to 1.16 g, with an average of 0.43 g, revealing a 2.98% difference from the reference value. Additionally, the log-standard deviation ranged from 0.15 to 1.57, with an average of 0.85, exhibiting a 5.63% difference from the reference value of 0.90. In Figure 11, the blue dashed line represents the reference value, the black line represents the 100,000-run average, and the other fine lines represent the fragility curves and frequency distributions from the 100,000-run analysis and the results of 10 ground motions are summarized in Table 11.

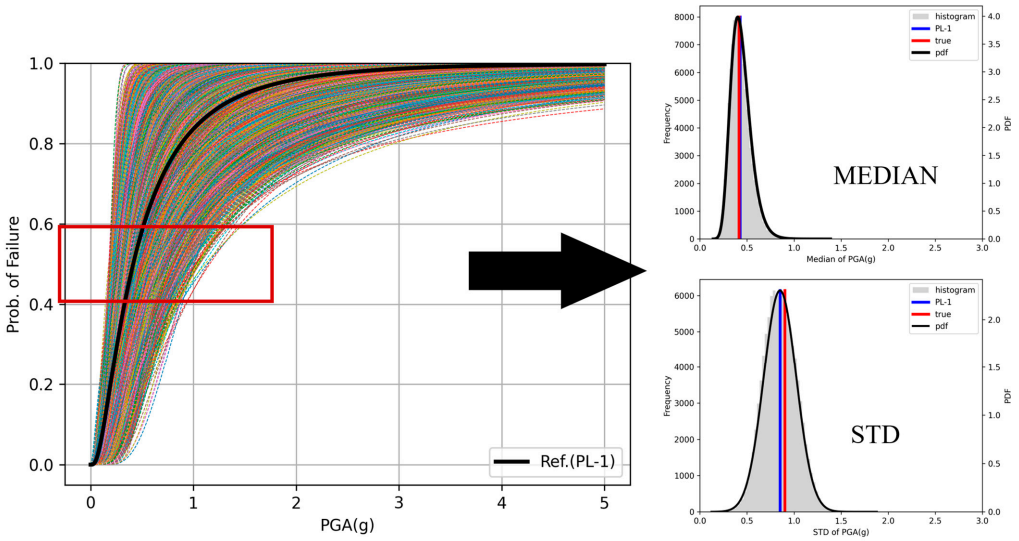

(**a**)

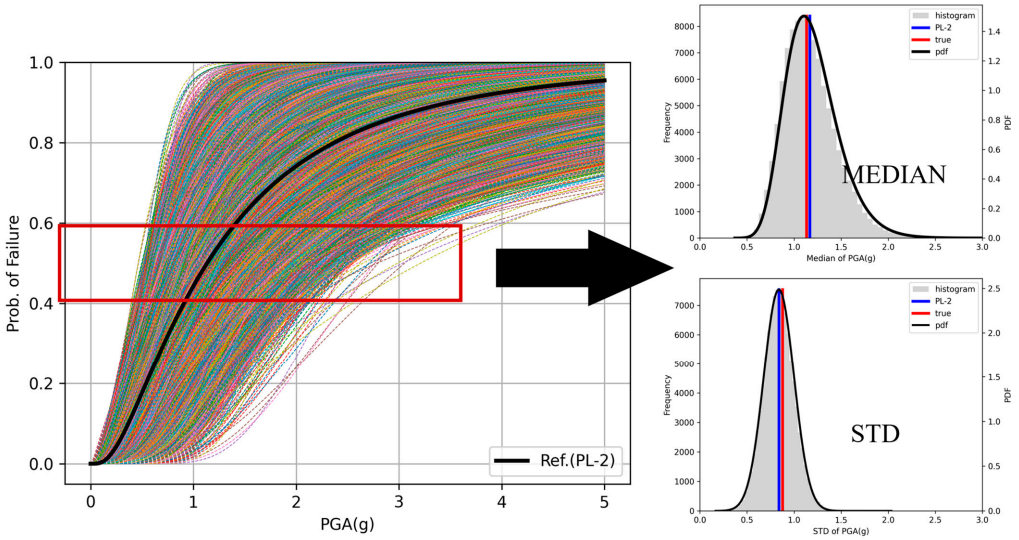

(**b**)

Figure 11. *Cont.*

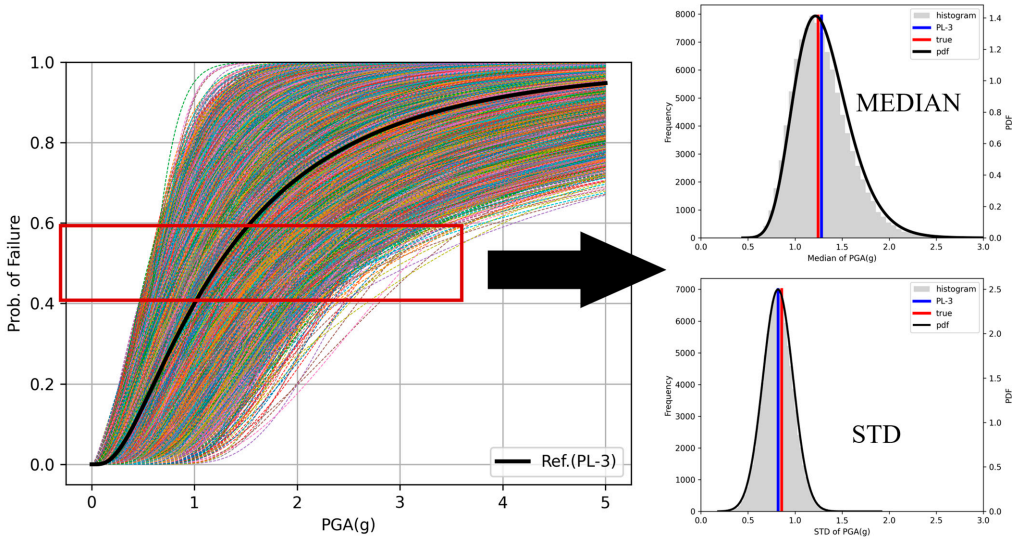

(**c**)

Figure 11. Seismic fragility curves and histograms of the 13-story building (N = 10). (**a**) Performance Level 1; (**b**) Performance Level 2; (**c**) Performance Level 3.

Table 11. Range of seismic fragility curve parameters of the 13-story building (N = 10).

Performance Level	**Median (g)**				**Difference (%)**
	Ref	**Min**	**Max**	**Avg**	
1—IO	0.4137	0.1748	1.1572	0.4261	2.9804
2—LS	1.1322	0.4623	3.2078	1.1667	3.0464
3—CP	1.2440	0.5546	3.2694	1.2795	2.8568
Performance Level	Log-standard deviation				Difference (%)
	Ref	Min	Max	Avg	
1—IO	0.9013	0.1535	1.5661	0.8506	5.6286
2—LS	0.8779	0.2072	1.6951	0.8388	4.4511
3—CP	0.8568	0.2292	1.5970	0.8186	4.4575

Tables 12–14 summarize the results for 30, 50, and 350 ground motions. Figure 12 illustrates the results for 30 ground motions.

Table 12. Range of seismic fragility curve parameters of the 13-story building (N = 30).

Performance Level	**Median (g)**				**Difference (%)**
	Ref	**Min**	**Max**	**Avg**	
1—IO	0.4137	0.2453	0.7232	0.4168	0.7312
2—LS	1.1322	0.7013	2.0056	1.1405	0.7315
3—CP	1.2440	0.7526	2.1098	1.2523	0.6734
Performance Level	Log-standard deviation				Difference (%)
	Ref	Min	Max	Avg	
1—IO	0.9013	0.5263	1.2547	0.8878	1.4969
2—LS	0.8779	0.5314	1.2453	0.8680	1.1231
3—CP	0.8568	0.5294	1.2067	0.8475	1.0868

Table 13. Range of seismic fragility curve parameters of the 13-story building (N = 50).

Performance Level	Median (g)				Difference (%)
	Ref	**Min**	**Max**	**Avg**	
1—IO	0.4137	0.2827	0.5855	0.4152	0.3517
2—LS	1.1322	0.7984	1.5579	1.1363	0.3652
3—CP	1.2440	0.8865	1.6866	1.2484	0.3537
Performance Level	Log-standard deviation				Difference (%)
	Ref	Min	Max	Avg	
1—IO	0.9013	0.6315	1.1376	0.8949	0.7168
2—LS	0.8779	0.6195	1.1253	0.8732	0.5263
3—CP	0.8568	0.6032	1.1228	0.8524	0.5202

Table 14. Range of seismic fragility curve parameters of the 13-story building (N = 350).

Performance Level	Median (g)				Difference (%)
	Ref	**Min**	**Max**	**Avg**	
1—IO	0.4137	0.3838	0.4451	0.4138	0.0168
2—LS	1.1322	1.0597	1.2098	1.1324	0.0156
3—CP	1.2440	1.1615	1.3226	1.2442	0.0156
Performance Level	Log-standard deviation				Difference (%)
	Ref	Min	Max	Avg	
1—IO	0.9013	0.8460	0.9562	0.9011	0.0272
2—LS	0.8779	0.8208	0.9311	0.8776	0.0238
3—CP	0.8568	0.8058	0.9060	0.8567	0.0197

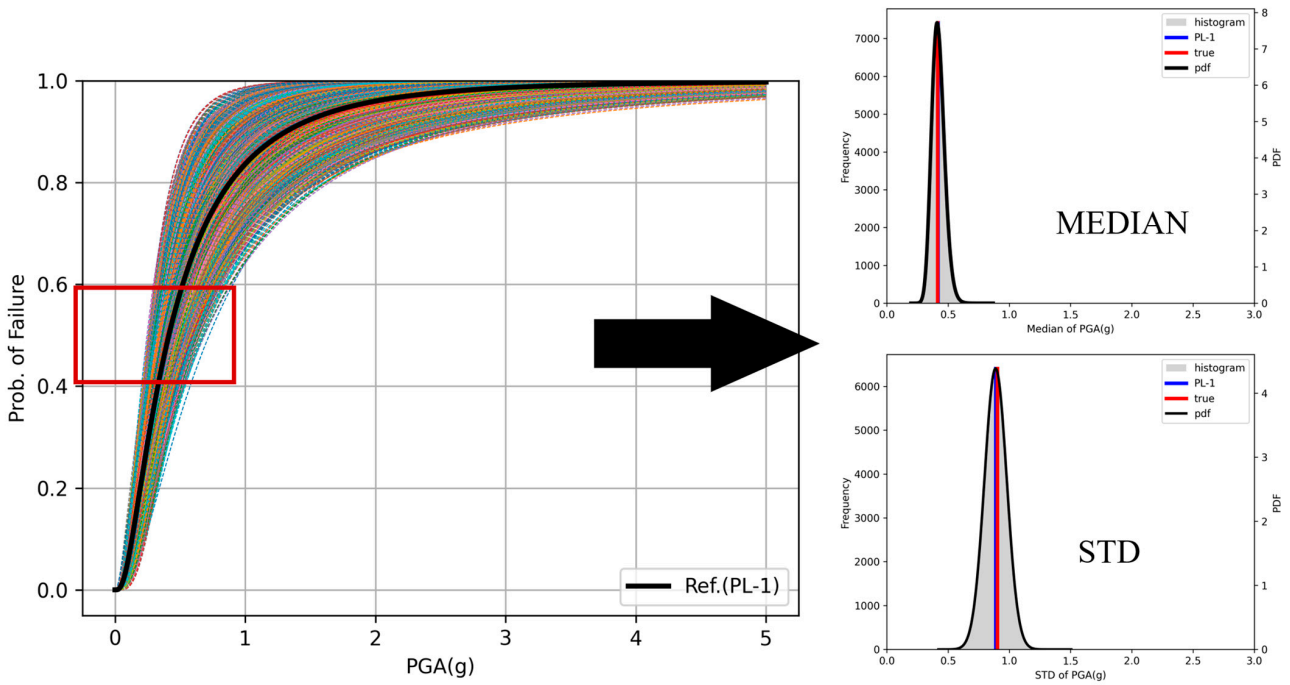

(**a**)

Figure 12. *Cont.*

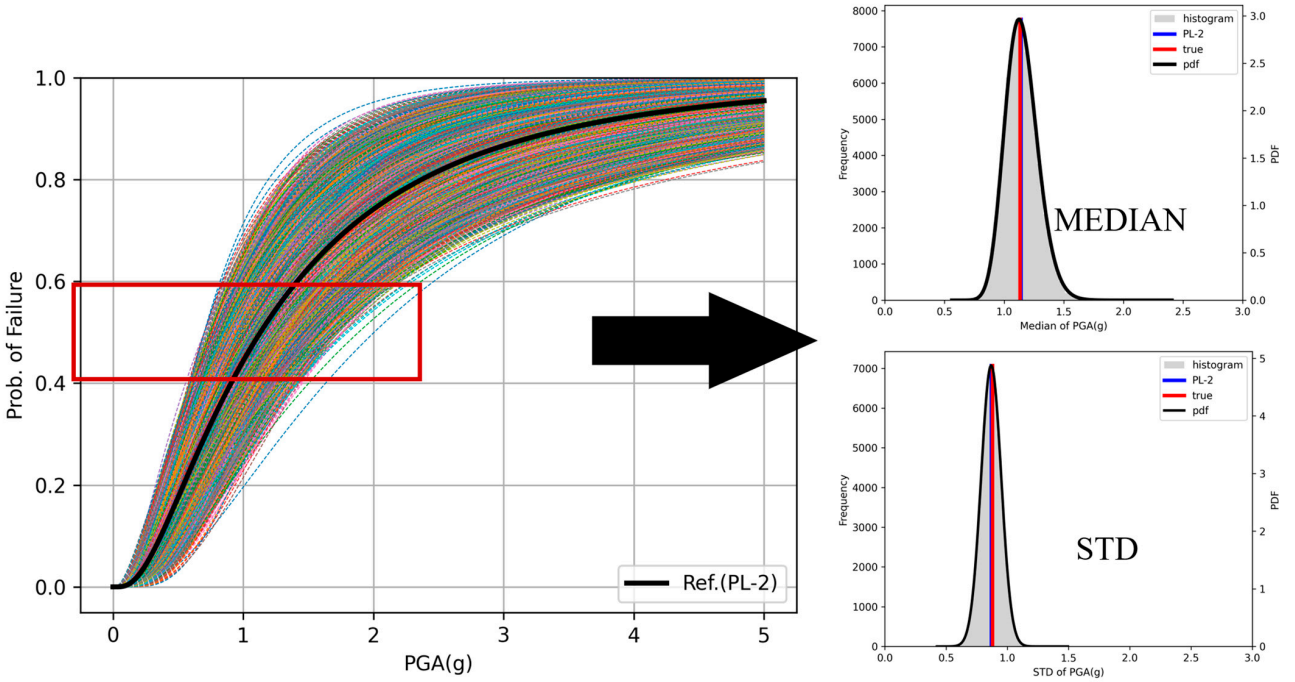

(**b**)

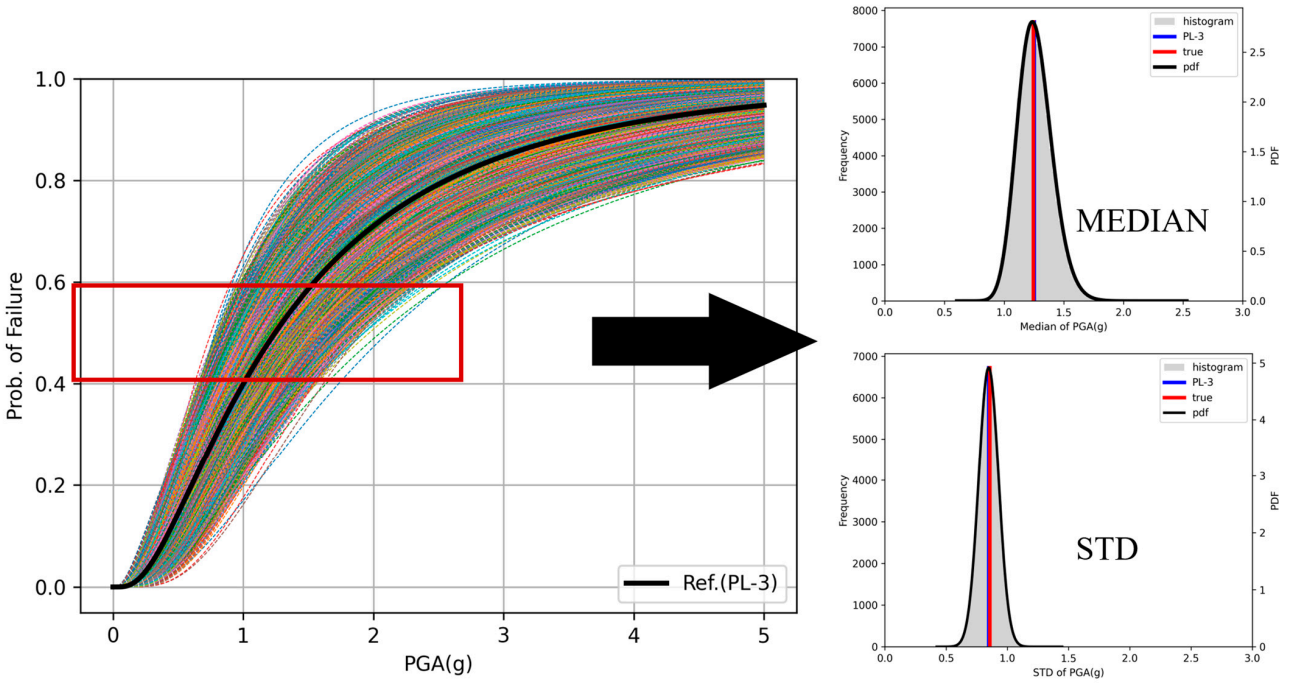

(**c**)

Figure 12. Seismic fragility curves and histograms of the 13-story building (N = 30). (**a**) Performance Level 1; (**b**) Performance Level 2; (**c**) Performance Level 3.

As the number of ground motions considered in deriving the seismic fragility curves increases, the overall difference from the reference values decreases despite slight differences for each performance level. This indicates that increasing the number of ground motions reduces the uncertainty in selecting the ground motions for fragility curve generation. Similar to the six-story example, Figure 13 illustrates the differences between the mean values of each fragility input variable and the reference values for the three performance levels.

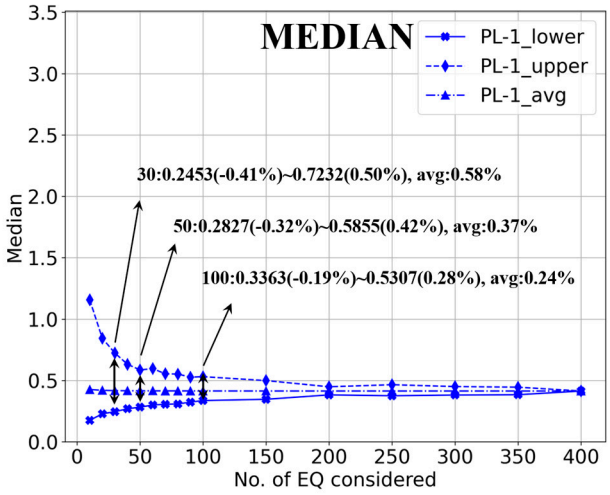

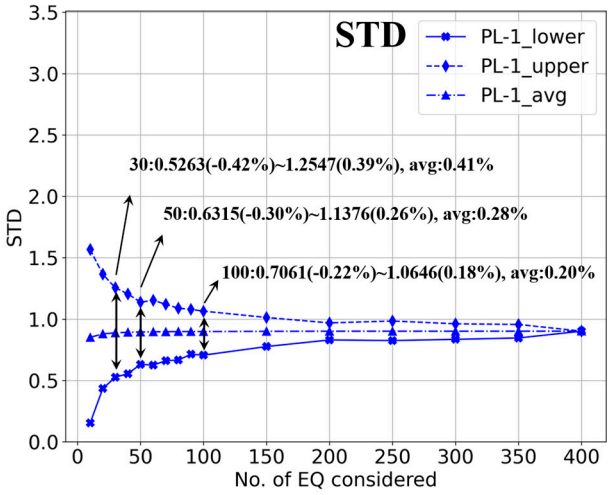

(**a**)

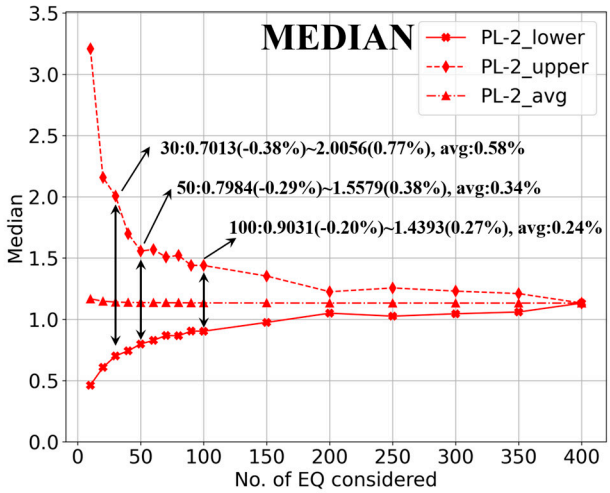

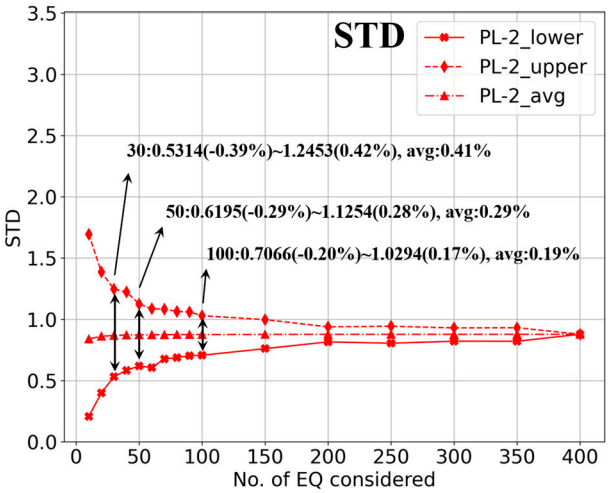

(**b**)

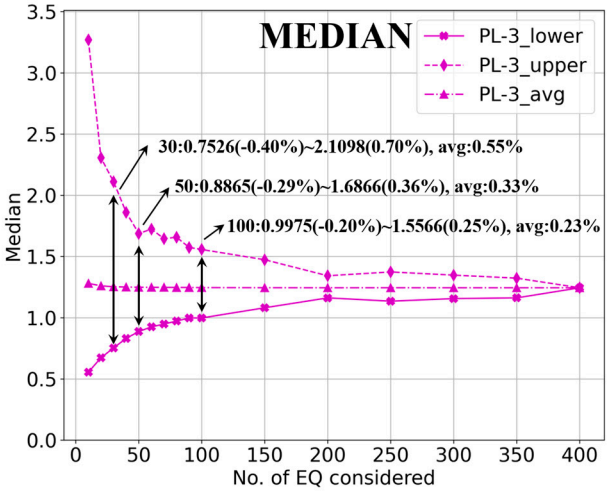

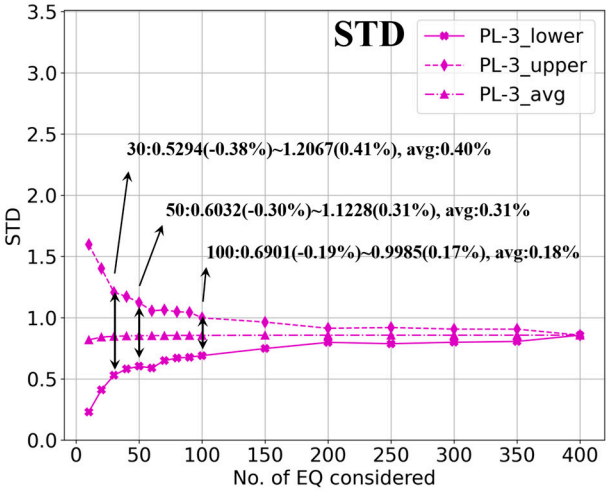

(**c**)

Figure 13. No. of ground motions vs. difference of the 13-story building. (**a**) Performance Level 1; (**b**) Performance Level 2; (**c**) Performance Level 3.

When deriving the seismic fragility curve for the 13-story example facility, the median and log-standard deviation values decreased as the number of ground motions considered increased when compared to the reference values. In cases with fewer than 30 ground motions, the rate of change was substantial in both example facilities. However, when 30 or more ground motions were used, the differences decreased at a relatively smaller rate as the number of ground motions increased.

5. Conclusions

A statistical analysis was conducted on the number of ground motions used to generate seismic fragility curves, which are widely used in damage assessments of structures affected by earthquakes. Using 400 ground motions, the study employed LHS, a sampling method commonly used in engineering experiments, to select various sets of ground motions. Seismic fragility curves were then generated for two example structures (a 6-story and a 13-story steel moment frame structure), using inter-story drift as the performance criterion for three performance levels.

The six-story structure, which has lower degrees of freedom, exhibited relatively small differences between the reference values for the median and log-standard deviation, whereas the 13-story structure, with higher degrees of freedom, exhibited relatively larger differences. However, when 50 or more ground motions were considered, the results for both example structures were similar. When comparing the median values, the difference from the reference values was less than 0.26% for the six-story structure and less than 0.36% for the 13-story structure. For the log-standard deviation, the difference was less than 0.73% and 0.59%, respectively, exhibiting minimal differences from the reference values, regardless of the degrees of freedom of the structures.

This study reveals that the ground motions considered when deriving seismic fragility curves based on inter-story drift are directly related to the structural response of the target facility. If the fragility curves are generated using relatively few ground motions, the uncertainty in the fragility curve variables increases, potentially distorting the results. Distorted results likely lead to inaccuracies in further analyses, such as seismic performance evaluations or damage cost estimations when using the fragility curve results. Therefore, considering an appropriate selection of ground motions and an adequate number of ground motions is important when generating seismic fragility curves. Finally, by increasing the number of ground motions, the amount of data available for deriving the input variables of the fragility curves also increases. This increase in data helps reduce uncertainty due to data limitations, improving the reliability of the fragility curve input variables.

Finally, this study has the limitation that it requires a high computational cost to provide more practical application through nonlinear time history analysis for various structural models. Also, the impact of the design characteristics and material properties of the two steel frame examples on seismic response and fragility assessment cannot be neglected. However, this study can provide information on the relationship between the number of input ground motions and seismic fragility curves, and it may be helpful to consider an appropriate number of ground motions for seismic fragility analysis.

Author Contributions: Conceptualization: S.P. and D.S.; formal analysis: S.P. and K.J.; funding acquisition: D.S. and J.K.; investigation: S.P. and J.K.; methodology: S.P.; project administration: D.S.; validation: K.J.; writing—original draft: S.P. and D.S.; writing—review and editing: K.J. and J.K. All authors have read and agreed to the published version of the manuscript.

Funding: This study was supported by the Ministry of Land, Infrastructure and Transport (MOLIT) (Project Number: KICT-20240043-001).

Institutional Review Board Statement: Not applicable.

Informed Consent Statement: Not applicable.

Data Availability Statement: The original contributions presented in this study are included in the article. Further inquiries can be directed to the corresponding authors.

Conflicts of Interest: The authors declare no conflicts of interest. The funders had no role in the design of the study; in the collection, analyses, or interpretation of data; in the writing of the manuscript; or in the decision to publish the results.

References

1. U.S. Geological Survey (USGS). Earthquake Hazards Program. Available online: https://www.usgs.gov/programs/earthquake-hazards (accessed on 20 June 2024).
2. Kennedy, R.P.; Ravindra, M.K. Seismic fragilities for nuclear power plant risk studies. *Nucl. Eng. Des.* **1984**, *79*, 47–68. [CrossRef]
3. EPRI. *Methodology for Developing Seismic Fragilities*; EPRI: Palo Alto, CA, USA, 1994.
4. Shinozuka, M.; Feng, M.Q.; Lee, J.; Naganuma, T. Statistical analysis of fragility curves. *J. Eng. Mech.* **2000**, *126*, 1224–1231. [CrossRef]
5. Porter, K.; Kennedy, R.; Bachman, R. Creating fragility functions for performance-based earthquake engineering. *Earthq. Spectra* **2007**, *23*, 471–489. [CrossRef]
6. Baker, J.W.; Allin Cornell, C.A. Spectral shape, epsilon and record selection. *Earthq. Eng. Struct. Dyn.* **2006**, *35*, 1077–1095. [CrossRef]
7. Baker, J.W. Efficient analytical fragility function fitting using dynamic structural analysis. *Earthq. Spectra* **2015**, *31*, 579–599. [CrossRef]
8. Park, H.S.; Nguyen, D.-D.; Lee, T.-H. Seismic fragilities of bridges and transmission towers considering recorded ground motions in South Korea. *J. Earthq. Eng. Soc. Korea* **2016**, *20*, 435–441. [CrossRef]
9. Jeon, S.-H.; Shin, D.-H.S.; Park, J.-H. Seismic fragility assessment for Korean high-rise non-seismic RC shear wall apartment buildings. *J. Earthq. Eng. Soc. Korea* **2020**, *24*, 293–303. [CrossRef]
10. Kim, J.; Kim, T. Seismic fragility function for existing low-rise piloti-type buildings reflecting damage from Pohang earthquake. *J. Earthq. Eng. Soc. Korea* **2021**, *25*, 251–259. [CrossRef]
11. Aldea, S.; Bazaez, R.; Astroza, R.; Hernandez, F. Seismic fragility assessment of Chilean skewed highway bridges. *Eng. Struct.* **2021**, *249*, 113300. [CrossRef]
12. Dumova-Jovanoska, E. Fragility curves for reinforced concrete structures in Skopje (Macedonia) region. *Soil. Dyn. Earthq. Eng.* **2000**, *19*, 455–466. [CrossRef]
13. Kappos, A.J.; Panagopoulos, G. Fragility curves for reinforced concrete buildings in Greece. *Struct. Infrastruct. Eng.* **2010**, *6*, 39–53. [CrossRef]
14. Su, L.; Li, X.; Jiang, Y. Comparison of Methodologies for Seismic Fragility Analysis of Unreinforced Masonry Buildings Considering Epistemic Uncertainty. *Eng. Struct.* **2020**, *205*, 110059. [CrossRef]
15. Blasi, G.; Perrone, D.; Aiello, M.A. Fragility curves for reinforced concrete frames with retrofitted masonry infills. *J. Build. Eng.* **2023**, *75*, 106951. [CrossRef]
16. Eads, L.; Miranda, E.; Krawinkler, H. An efficient method for estimating the collapse risk of structures in seismic regions. *Earthq. Eng. Struct. Dyn.* **2013**, *42*, 25–41. [CrossRef]
17. Ruggieri, S.; Porco, F.; Uva, G.; Vamvatsikos, D. Two frugal options to assess class fragility and seismic safety for low-rise reinforced concrete school buildings in Southern Italy. *Bull. Earthq. Eng.* **2021**, *19*, 1415–1439. [CrossRef]
18. Nettis, A.; Raffaele, D.; Uva, G. Seismic risk-informed prioritization of multi-span RC girder bridges considering knowledge-based uncertainty. *Bull. Earthq. Eng.* **2024**, *22*, 693–729. [CrossRef]
19. Li, H.; Li, L.; Zhou, G.; Xu, L. Effects of various modeling uncertainty parameters on the seismic response and seismic fragility estimates of the aging highway bridges. *Bull. Earthq. Eng.* **2020**, *18*, 6337–6373. [CrossRef]
20. Bovo, M.; Buratti, N. Evaluation of the variability contribution due to epistemic uncertainty on constitutive models in the definition of fragility curves of RC frames. *Eng. Struct.* **2019**, *188*, 700–716. [CrossRef]
21. Roueche, D.B.; Prevatt, D.O.; Lombardo, F.T. Epistemic uncertainties in fragility functions derived from post-disaster damage assessments. *ASCE-ASME J. Risk Uncertain. Eng. Syst. Part A Civ. Eng.* **2018**, *4*, 04018015. [CrossRef]
22. Vamvatsikos, D.; Cornell, C.A. Incremental dynamic analysis. *Earthq. Eng. Struct. Dyn.* **2002**, *31*, 491–514. [CrossRef]
23. Vamvatsikos, D.; Cornell, C.A. Applied incremental dynamic analysis. *Earthq. Spectra* **2004**, *20*, 523–553. [CrossRef]
24. Federal Emergency Management Agency (FEMA). *Quantification of Building Seismic Performance Factors*; Federal Emergency Management Agency: Washington, DC, USA, 2009.
25. Nakamura, T.; Naganuma, T.; Shizuma, T.; Shinozuka, M. A study on failure probability of highway bridge by earthquake based on statistical method. In Proceedings of the 10th Japanese Earthquake Engineering Symposium, Tokyo, Japan, 25 November 1998.
26. Yi, S.; Papaknstantinou, K.G.; Andriotis, C.P.; Song, J. Appraisal and mathematical properties of fragility analysis models. In Proceedings of the 13th International Conference on Structural Safety and Reliability (ICOSSAR 2021), Shanghai, China, 21–25 June 2021.
27. Jalayer, F.; Cornell, C.A. Alternative non-linear demand estimation methods for probability-based seismic assessments. *Earthq. Eng. Struct. Dyn.* **2009**, *38*, 951–972. [CrossRef]
28. Kunnath, S.K.; Nghiem, Q.; El-Tawil, S. Modeling and response prediction in performance-based seismic evaluation: Case studies of instrumented steel moment-frame buildings. *Earthq. Spectra* **2004**, *20*, 883–915. [CrossRef]

29. Kalkan, E.; Kunnath, S.K. Effects of fling step and forward directivity on seismic response of buildings. *Earthq. Spectra* **2006**, *22*, 367–390. [CrossRef]
30. Kalkan, E.; Chopra, A.K. *Practical Guidelines to Select and Scale Earthquake Records for Nonlinear Response History Analysis of Structures*; Open-File Report 2010-1068; United States Geological Survey: Asheville, NC, USA, 2010; ISBN 9781495381683.
31. Anderson, J.C.; Bertero, V.V. *Implications of the Landers and Big Bear Earthquakes on Earthquake Resistant Design of Structures [Report]*; Earthquake Engineering Research Center, University of California at Berkeley: Berkeley, CA, USA, 1997.
32. McKenna, F.T. Object-Oriented Finite Element Programming: Frameworks for Analysis, Algorithms and Parallel Computing. Ph.D. Thesis, University of California Berkeley, Berkeley, CA, USA, 1997.
33. Rezaei, S.; Akbari Hamed, A.; Basim, M.C. Seismic performance evaluation of steel structures equipped with dissipative columns. *J. Build. Eng.* **2020**, *29*, 101227. [CrossRef]
34. Dimov, I.T. *Monte Carlo Methods for Applied Scientists*; World Scientific: Singapore, 2007; ISBN 978-981-02-2329-8.
35. Mckay, M.D.; Beckman, R.J.; Conover, W.J. Comparison of three methods for selecting values of input variables in the analysis of output from a computer code. *Technometrics* **1979**, *21*, 239–245. [CrossRef]
36. Helton, J.C.; Davis, F.J. Latin hypercube sampling and the propagation of uncertainty in analyses of complex systems. *Reliab. Eng. Syst. Saf.* **2003**, *81*, 23–69. [CrossRef]
37. Uang, C.-M. *Performance of a 13-Story Steel Moment-Resisting Frame Damaged in the 1994 Northridge Earthquake [Report]*; Structural Systems Research Project; Structural Systems Research, University of California: San Diego, CA, USA, 1995.

Disclaimer/Publisher's Note: The statements, opinions and data contained in all publications are solely those of the individual author(s) and contributor(s) and not of MDPI and/or the editor(s). MDPI and/or the editor(s) disclaim responsibility for any injury to people or property resulting from any ideas, methods, instructions or products referred to in the content.